The catalytic core of DEMETER guides active DNA demethylation in *Arabidopsis*

Changqing Zhang[a,b,1], Yu-Hung Hung[a,b,1], Hyun Jung Rim[c,d,e,1], Dapeng Zhang[f], Jennifer M. Frost[g,2], Hosub Shin[c,d,e], Hosung Jang[c,d,e], Fang Liu[a,b,h], Wenyan Xiao[f], Lakshminarayan M. Iyer[i], L. Aravind[i], Xiang-Qian Zhang[a,b,j,3], Robert L. Fischer[g,3], Jin Hoe Huh[c,d,e,3], and Tzung-Fu Hsieh[a,b,3]

[a]Department of Plant and Microbial Biology, North Carolina State University, Raleigh, NC 27695; [b]Plants for Human Health Institute, North Carolina State University, North Carolina Research Campus, Kannapolis, NC 28081; [c]Department of Plant Science, Seoul National University, 08826 Seoul, Republic of Korea; [d]Research Institute for Agriculture and Life Sciences, Seoul National University, 08826 Seoul, Republic of Korea; [e]Plant Genomics and Breeding Institute, Seoul National University, 08826 Seoul, Republic of Korea; [f]Department of Biology, St. Louis University, St. Louis, MO 63103; [g]Department of Plant and Microbial Biology, University of California, Berkeley, CA 94720; [h]State Key Laboratory for Conservation and Utilization of Subtropical Agro-Bioresources, College of Agriculture, Guangxi University, 530004 Nanning, China; [i]National Center for Biotechnology Information, National Library of Medicine, National Institutes of Health, Bethesda, MD 20894; and [j]College of Forestry and Landscape Architecture, South China Agricultural University, 510642 Guangzhou, China

Contributed by Robert L. Fischer, July 12, 2019 (sent for review April 29, 2019; reviewed by James J. Giovannoni and Julie A. Law)

The *Arabidopsis* DEMETER (DME) DNA glycosylase demethylates the maternal genome in the central cell prior to fertilization and is essential for seed viability. DME preferentially targets small transposons that flank coding genes, influencing their expression and initiating plant gene imprinting. DME also targets intergenic and heterochromatic regions, but how it is recruited to these differing chromatin landscapes is unknown. The C-terminal half of DME consists of 3 conserved regions required for catalysis in vitro. We show that this catalytic core guides active demethylation at endogenous targets, rescuing *dme* developmental and genomic hypermethylation phenotypes. However, without the N terminus, heterochromatin demethylation is significantly impeded, and abundant CG-methylated genic sequences are ectopically demethylated. Comparative analysis revealed that the conserved DME N-terminal domains are present only in flowering plants, whereas the domain architecture of DME-like proteins in nonvascular plants mainly resembles the catalytic core, suggesting that it might represent the ancestral form of the 5mC DNA glycosylase found in plant lineages. We propose a bipartite model for DME protein action and suggest that the DME N terminus was acquired late during land plant evolution to improve specificity and facilitate demethylation at heterochromatin targets.

gene imprinting | active DNA demethylation | endosperm development | epigenetic reprogramming | *Arabidopsis thaliana*

DNA methylation is a covalent modification that influences the transcription of nearby genes and regulates important processes in eukaryotic genomes, including cell differentiation, transposable element (TE) silencing, and genomic imprinting (1, 2). Plant DNA methylation occurs in CG, CHG, and CHH sequence contexts (H = A, C, or T) and is targeted primarily to TEs. Flowering plants and mammals can also exhibit gene body methylation (gbM) in the CG context, generally in constitutively expressed genes, but the function of gbM is not fully understood (3, 4).

DNA methylation homeostasis is essential for genome stability, notably in maintaining TE silencing, and for the stable inheritance of epigenetic information (5, 6). In plants, this is achieved by maintenance and de novo DNA methylation, as well as by active DNA demethylation (1, 7, 8). Active DNA demethylation is catalyzed by a family of DNA glycosylases, including REPRESSOR OF SILENCING 1 (ROS1), DEMETER (DME), and DEMETER-LIKE 2 (DML2) and DML3, through a base excision repair pathway (9–11). However, epigenetic profiles are dynamic in response to biotic and abiotic stress and during reproduction and development. Similar to mammals, flowering plants require epigenetic reprogramming during gamete formation, as characterized by extensive DNA demethylation in *Arabidopsis* by DME (12–14).

DME encodes a bifunctional 5mC DNA glycosylase/lyase that is essential for reproduction (9, 15). Paralogs ROS1, DML2, and DML3 function primarily in the sporophyte to counteract the spread of DNA methylation mediated by RNA-dependent DNA methylation (16, 17). The A, glycosylase, and B regions of the C-terminal half of DME are conserved among the DME/ROS1 DNA glycosylase clade and are absolutely required for DME 5mC excision in vitro, composing the catalytic core for its enzymatic activity (9, 15). DME acts primarily in the central cell and the vegetative nucleus (15, 18, 19). The vegetative nucleus contributes to germination and growth of the pollen tube, which

Significance

Flowering plants reproduce via a unique double-fertilization event, producing the zygote and the nutritive endosperm. The genome of the central cell, the precursor of the endosperm, undergoes extensive demethylation prior to fertilization. This epigenetic reconfiguration, directed by the DEMETER (DME) glycosylase at thousands of loci in *Arabidopsis*, differentiates the epigenetic landscapes of parental genomes and establishes parent of origin-specific expression of many imprinted genes in endosperm essential for seed development. However, how DME is targeted to various locations remains unknown. Here we show that the multidomain DME is organized into 2 functional regions: the C-terminal region, which guides localization and catalysis, and the N-terminal region, which likely recruits chromatin remodelers to facilitate demethylation within heterochromatin.

Author contributions: C.Z., Y.-H.H., W.X., R.L.F., J.H.H., and T.-F.H. designed research; C.Z., Y.-H.H., H.J.R., D.Z., H.S., H.J., F.L., and X.-Q.Z. performed research; C.Z., Y.-H.H., H.J.R., D.Z., J.M.F., L.M.I., L.A., X.-Q.Z., J.H.H., and T.-F.H. analyzed data; and J.M.F., R.L.F., J.H.H., and T.-F.H. wrote the paper.

Reviewers: J.J.G., US Department of Agriculture Agricultural Research Service Robert W. Holley Center and Boyce Thompson Institute for Plant Research; and J.A.L., Salk Institute for Biological Studies.

The authors declare no conflict of interest.

Data deposition: The data reported in this paper have been deposited in the Gene Expression Omnibus (GEO) database, www.ncbi.nlm.nih.gov/geo/ (accession no. GSE130559).

[1]C.Z., Y.-H.H., and H.J.R. contributed equally to this work.

[2]Present address: Blizard Institute, Barts and The London School of Medicine and Dentistry, Queen Mary University of London, E1 2AT London, United Kingdom.

[3]To whom correspondence may be addressed. Email: aacrav@163.com, rfischer@berkeley.edu, huhjh@snu.ac.kr, or thsieh3@ncsu.edu.

This article contains supporting information online at www.pnas.org/lookup/suppl/doi:10.1073/pnas.1907290116/-/DCSupplemental.

Published online August 13, 2019.

delivers the sperm cells to the female gametophyte. Following double fertilization, the egg and central cell develop into the embryo and the nutritive endosperm, respectively, the latter of which accumulates starch, lipids, and storage proteins to nourish the developing embryo. The endosperm is the site of plant genomic imprinting, resulting from allelic inheritance of differential epigenetic states (20–22). DNMT1 homolog MET1-mediated DNA methylation and DME-mediated demethylation are important regulators of plant gene imprinting. For example, DME demethylation is required to activate *MEA*, *FIS2*, and *FWA* expression in the central cell, which persists in the endosperm, while MET1 maintains the silencing of *FIS2* and *FWA* paternal alleles (20–22). Imprinting is essential for reproduction in *Arabidopsis*, and seeds that inherit a maternal *dme* allele abort due to failure to activate *MEA* and *FIS2*, essential components of the Polycomb Repressive Complex 2 (PRC2) required for seed viability (20–22).

Although DME preferentially targets small AT-rich and nucleosome-poor euchromatic transposons, it also demethylates intergenic and heterochromatin targets (13). How DME is recruited to target sites with various chromatin structures is unknown, although the Facilitates Chromatin Transactions (FACT) histone chaperone is required at heterochromatic targets and some imprinted loci (23, 24). Other than the glycosylase domain, the catalytic core region of DME contains multiple conserved globular domains of unknown function.

Here we show that expressing a nuclear-localized DME catalytic region controlled by a native *DME* promoter complements *dme* seed abortion and pollen germination defects and partially rescues the DNA hypermethylation phenotype in endosperm. Our DNA methylation analysis revealed that the majority of canonical DME target sites are demethylated by the catalytic core, indicating that this region is sufficient to direct DME localization. However, without the N-terminal region, the degree of demethylation is reduced, and demethylation of heterochromatin targets is particularly impeded. In addition, we observed prevalent ectopic demethylation, specifically at genic sequences, by the catalytic core. Thus, the N-terminal region of DME is likely needed for the full breadth and depth of demethylation and to prevent gene body demethylation. We show that the N-terminal conserved domains are specific to the angiosperm lineage, acquired late during land plant evolution, potentially to ensure robust demethylation in nucleosome-rich heterochromatin targets.

Results

Nuclear-Localized Catalytic Core of DME Rescues *dme* Developmental Defects. *DME* produces at least 2 alternatively spliced variants, encoding 2 hypothetical polypeptides of 1,729 (DME.1) and 1,987 (DME.2) amino acids in length (11, 15). The amino acid positions denoted in this study correspond to DME.2, the predominant isoform expressed in floral tissues (18). First, we detailed the domain structure and predicted characteristics of the catalytic and noncatalytic regions of the DME protein. The N-terminal half of DME consists of a large portion of unstructured, low-complexity sequences (amino acids 364–947; Fig. 1*A*), a stretch of basic amino acid-rich repeats (amino acids 291–363; basic stretch) known to direct nuclear localization (15), and a 120-aa N-terminal domain (amino acids 1–120, DemeN) of unknown function present only among the angiosperm DME/ROS1-like proteins. Within the DemeN domain is a sWIPxTPxKs motif that is highly conserved (*SI Appendix*, Fig. S1) but is absent in the shorter DME.1 isoform. This motif has a hydrophobic core and may mediate protein–protein interactions and/or be subjected to posttranslational modification (i.e., phosphorylation or methylation at the lysine residue). The basic stretch region is highly conserved among angiosperm DME-like proteins and is reminiscent of the AT-hook motifs that can bind DNA in a non–sequence-specific manner (25), suggesting that the basic stretch might also bind DNA along with directing DME to the nucleus.

It was determined that the C-terminal half of DME (amino acids 936–1987; hereinafter the DME^{CTD}) constitutes the catalytic core for 5mC excision in vitro (9, 26). This core contains the glycosylase domain of the HhH (helix-hairpin-helix) motif, followed by the [4Fe-4S] cluster loop (FCL) motif (27). The conserved B region contains an RNA recognition motif fold (RRMF) and a divergent, circularly permuted version of a methylated CpG-discriminating CXXC domain (27). The presence of the permuted CXXC and RRMF raises the possibility that the enzymatic core might contain intrinsic targeting information (28, 29). To test this possibility, we investigated whether DME^{CTD} can rescue the *dme* seed abortion phenotype when expressed by an endogenous *DME* promoter. A classical SV40 nuclear localization signal (NLS) (PKKKPKV) was included to ensure robust nuclear localization (Fig. 1*A*). The

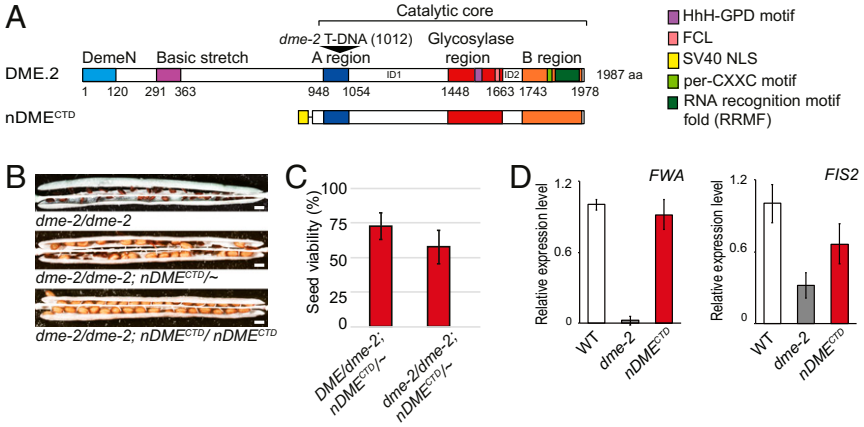

Fig. 1. Complementation results. (*A*) Domain architecture and the positions of conserved domains along DME protein. nDME^{CTD} is the construct used for complementation and methylome analyses. (*B*) In *dme-2/dme-2* siliques, >99% of seeds are aborted. A single copy of the *nDME^{CTD}* transgene reduces seed abortion to 50%, and in the *dme-2/dme-2; nDME^{CTD}/nDME^{CTD}* siliques, all seeds develop normally. (Scale bar: 0.5 mm.) (*C*) Percentages of viable seeds in *DME/dme-2* or in *dme-2/dme-2* plants that were complemented by *nDME^{CTD}* transgene. Error bars represent SD. (*D*) The *nDME^{CTD}* transgene restores DME target gene *FWA* and *FIS2* expression. WT: Col-0; nDME^{CTD}: *dme-2/dme-2; nDME^{CTD}/nDME^{CTD}*; *dme-2*: *dme-2* homozygotes. Total RNA was isolated from stage F1 to F12 floral buds.

resulting transgene, $nDME^{CTD}$, was transformed into *DME*/*dme-2* heterozygous Col-*gl* plants. Self-pollinated *DME*/*dme-2* plants produce 50% viable (inherited *DME* maternal allele) and 50% aborted (inherited *dme-2* maternal allele) F1 seeds. In contrast, transgenic lines that are *DME*/*dme-2* and hemizygous for a single-locus $nDME^{CTD}$ transgene produced a 3:1 ratio of viable to aborted F1 seeds when self-pollinated (1,292:439, 3:1, $\chi^2 = 0.12$, $P > 0.7$; *SI Appendix*, Table S1), indicating that $nDME^{CTD}$ fully complemented the *dme* seed abortion phenotype. When $nDME^{CTD}$ was transformed into *dme-2*/*dme-2* homozygous plants (*SI Appendix*, *Materials and Methods*), the T1 transgenic lines (*dme-2*/*dme-2*;$nDME^{CTD}$/~) displayed a 50% to 75% rate of viable seeds when self-pollinated (*SI Appendix*, Table S1), compared with selfed nontransformed *dme-2*/*dme-2* plants, which bear <0.05% viable seeds, again indicating full seed abortion complementation by $nDME^{CTD}$ (Fig. 1 *B* and *C* and *SI Appendix*, Table S1). These results show that $nDME^{CTD}$ rescues the *dme-2* seed abortion phenotype. Since seed abortion is partially due to defects in activating imprinted *PRC2* genes (22), we used qRT-PCR to measure the expression of PRC2 subunit *FIS2* and of *FWA*, whose maternal expression is enabled by DME-mediated DNA demethylation, and found that $nDME^{CTD}$ restored the expression of these genes (Fig. 1*D*).

DME is also expressed in the vegetative cells of pollen, and mutations in *DME* reduce pollen germination, resulting in lower transmission of the paternal *dme* allele in certain ecotypes (19). Under our growth conditions, when *DME*/*dme-2* heterozygous Col-*gl* plants were self-pollinated, approximately 20% to 30% (compared with the expected 50% when the *dme-2* allele is normally transmitted) of the F1 progeny were *dme-2* heterozygotes (*SI Appendix*, Table S2). To test whether $nDME^{CTD}$ can rescue the *dme* pollen phenotype, we pollinated wild-type Col-0 with pollens from transgenic lines that are *dme-2* homozygous and hemizygous for the $nDME^{CTD}$ transgene (*dme-2*/*dme-2*; $nDME^{CTD}$/~ lines with ~50% seed abortion rates; *SI Appendix*, Table S1). If $nDME^{CTD}$ does not complement *dme-2* pollen germination defects, we would expect roughly one-half of the F1 progeny to carry the $nDME^{CTD}$ transgene (hygromycin-resistant), because mutant pollen with or without the transgene would germinate with equal frequency. Instead, we observed that 65% to 90% of the F1 progeny are hygromycin-resistant (resistant:sensitive = 190:52, 1:1, $\chi^2 = 79.69$, $P = 7.3E^{-19}$; *SI Appendix*, Table S3), indicating that $nDME^{CTD}$ rescues *dme-2* pollen defects. These results show that $nDME^{CTD}$ can rescue the *dme* developmental phenotype, indicating that DME targeting information is contained within the catalytic core.

Canonical DME Target Loci Are Demethylated by $nDME^{CTD}$. The molecular cause of DME mutant phenotypes is a loss of DME-mediated DNA demethylation. To test the extent of $nDME^{CTD}$ complementation, we compared the methylome of the $nDME^{CTD}$-complemented endosperm with the methylomes of wild-type and *dme-2* endosperm (13). $nDME^{CTD}$-complemented endosperm methylomes from 3 independent lines (*dme-2*/*dme-2*, $nDME^{CTD}$/$nDME^{CTD}$) were generated and the reads combined for downstream analyses. Pearson correlation coefficients between independent lines showed that they were highly concordant (*SI Appendix*, Table S4). We compared the differentially methylated regions (DMRs) between *dme-2* and wild-type endosperm (canonical DME targets; $n = 8{,}872$), and the DMRs between *dme-2* and $nDME^{CTD}$-complemented endosperm ($nDME^{CTD}$ targets; $n = 8{,}939$). Looking genome-wide, but excluding all DME and $nDME^{CTD}$ targets, the Pearson correlation coefficients between our combined independent lines and the previously published wild-type and *dme-2* endosperm datasets ranged between 0.92 and 0.94 (*SI Appendix*, Table S5), indicating a high level of concordance between the methylomes used in this study.

We found several DME-regulated imprinting control regions of maternally and paternally expressed genes (MEGs and PEGs, respectively) to be hypomethylated in the $nDME^{CTD}$-complemented endosperm compared with *dme-2* endosperm (*SI Appendix*, Fig. S2), suggesting that $nDME^{CTD}$ is active at these loci. CG methylation does not return to wild-type levels, however, indicating that the genome is demethylated to a lesser degree by $nDME^{CTD}$ than by wild-type DME (Fig. 2*A* and *SI Appendix*, Fig. S3*A*). The DME and $nDME^{CTD}$ DMRs largely overlap (Fig. 2*B*), and for the DMRs that appear unique to DME, the same regions are also demethylated by $nDME^{CTD}$ (Fig. 2*C*, black solid line trace), but to a reduced degree (the solid black peak is on the left of the dotted peak) that falls below our DMR cutoff (fractional CG methylation difference ≥0.3; $P < 10^{-10}$, Fisher's exact test). The shared DMRs are also slightly less demethylated in $nDME^{CTD}$-complemented endosperm compared with wild-type endosperm (Fig. 2*D*, red trace the left of the black trace). Taken together, these data show that $nDME^{CTD}$ rescues the *dme* hypermethylation phenotype, but only partially. As far as we could ascertain, this was not a result of lower transgene expression, since qRT-PCR analyses of endosperm tissue showed abundant expression of $nDME^{CTD}$ (*SI Appendix*, Fig. S3*B*).

To investigate whether chromatin features influence $nDME^{CTD}$ demethylation, we assessed histone marks and genomic characteristics (30) in target sites that are $nDME^{CTD}$-unique, DME-unique, or shared between the 2 types. Compared with $nDME^{CTD}$-DME shared DMRs, DME-unique target sites are highly enriched for heterochromatin states 8 and 9 (χ^2 test, $P = 8.29E^{-7}$, kb as unit of length; Fig. 2*E*). $nDME^{CTD}$ DMRs (unique and shared) are enriched for open chromatin states (χ^2 test, $P = 4.46E^{-117}$), but show significant reductions in heterochromatic chromatin states 8 and 9 compared with DME DMRs (χ^2 test, $P = 8.3.45E^{-153}$; Fig. 2*E*). Thus, $nDME^{CTD}$ demethylates poorly at heterochromatic loci and preferentially targets euchromatin.

Reduced Demethylation Efficiency at Long Heterochromatic Target Sites by $nDME^{CTD}$. Longer DME DMRs almost exclusively reside in heterochromatin (86.3% of 1–1.5 kb and 95.5% of ≥1.5 kb; Fig. 3*A*). We postulate that this is due to the dense methylation associated with heterochromatin, which may result in longer stretches of DNA demethylation during DME occupancy at these sites. Interestingly, the number of long DMRs is dramatically reduced in $nDME^{CTD}$-complemented endosperm (Fig. 3 *A* and *B*). This reduction in the number of longer DMRs was not due to a lack of $nDME^{CTD}$ targeting to these sites, since the partial demethylation characteristic of $nDME^{CTD}$ activity occurred in all targets regardless of their length (*SI Appendix*, Fig. S3*C*). However, when we analyzed the length of the $nDME^{CTD}$ demethylated regions, we found that it produced much shorter DMRs in the heterochromatin targets (*SI Appendix*, Fig. S4). For example, there are 250 DME DMRs longer than 1.5 kb (median length, 1.9 kb). Among these, 165 are also DMRs of $nDME^{CTD}$ but are much shorter (median length, 400 bp) (Fig. 3 *C* and *D*). Thus, removal of the DME N-terminal region significantly reduced the extent of demethylation in these long targets.

The histone chaperone FACT complex is required for demethylation of approximately one-half of DME targets in *Arabidopsis*, particularly those in heterochromatin (23). DME colocalizes with SPT16 (the larger FACT subunit) in an in vivo bimolecular fluorescence complementation assay, suggesting that DME might recruit the FACT complex to these heterochromatic loci (23). Of the 250 long DME DMRs, 87% of them require FACT, raising the possibility that $nDME^{CTD}$ might be defective in recruiting FACT. To test this hypothesis, we examined how $nDME^{CTD}$ demethylates FACT-dependent vs. FACT-independent loci. In wild-type endosperm, both target groups are demethylated to a similar degree (Fig. 3 *E*, blue and green traces with similar shape and peak location). In $nDME^{CTD}$-complemented

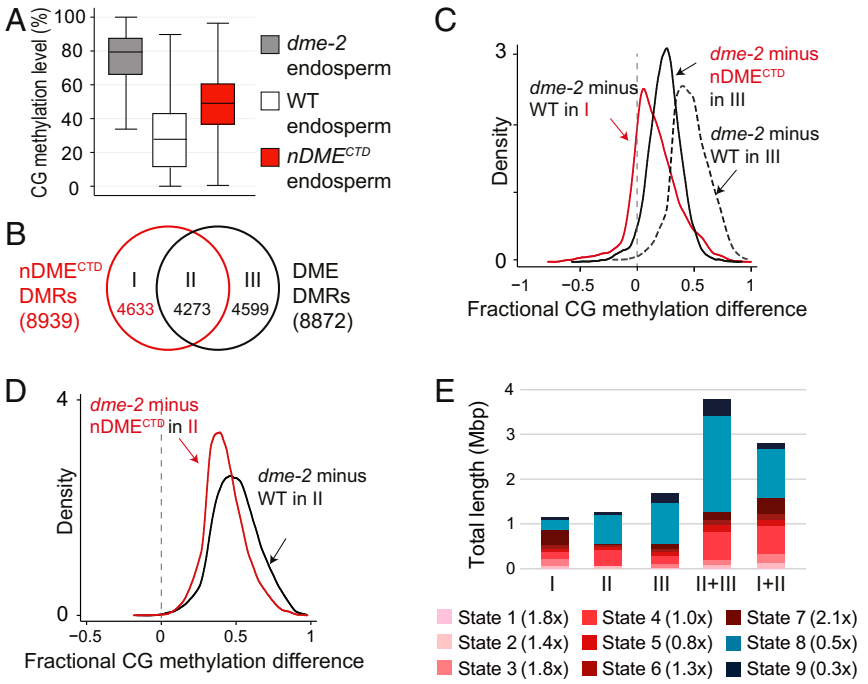

Fig. 2. Methylome analysis. (*A*) Boxplot of CG methylation of canonical DME target sites in *dme-2* mutant (gray), wild-type (white), or *nDME*^{CTD}-complemented (red) endosperm. (*B*) Venn diagram depicting unique and shared regions and loci numbers between DME and nDME^{CTD} DMRs. (*C*) Kernel density plots of CG methylation differences between *dme-2* and wild-type endosperm (black dotted trace), or between *dme-2* and *nDME*^{CTD}-complemented endosperm (black trace), for DME unique DMRs and CG methylation difference between *dme-2* and wild-type endosperm for nDME^{CTD}-unique DMRs (orange trace). (*D*) Kernel density plots of CG methylation differences between *dme-2* and *nDME*^{CTD}-complemented endosperm (black trace), or between *dme-2* and wild-type endosperm (orange trace), within the DME and nDME^{CTD} shared DMRs that completely overlap. (*E*) Chromatin state distribution, and total length covered, within nDME^{CTD}-unique (I), nDME^{CTD}-DME shared (II), DME-unique (III), DME-all (II+III), and nDME^{CTD}-all (I+II) DMRs. States 1 to 7 correspond to euchromatin, and states 8 and 9 correspond to AT- and GC-rich heterochromatin, respectively. The numbers in the parentheses show fold changes (total length) in nDME^{CTD} relative to DME DMRs.

endosperm, FACT-independent loci are only slightly less demethylated compared with wild-type endosperm (Fig. 3 *E*, orange trace moderately shifted to the left of blue and green traces). In contrast, demethylation at FACT-dependent loci is more severely impeded (Fig. 3 *E*, magenta trace). These results support a model in which DME recruits FACT via its N-terminal region to make heterochromatic targets accessible.

Prevalent Ectopic Gene Body Demethylation by nDME^{CTD}. We identified a set of new DMRs unique to nDME^{CTD}, which we term "ectopic" targets (Fig. 2*B*). The CG methylation difference between *dme-2* and wild-type endosperm for these DMRs is minimal but not absent (Fig. 2 *C*, the red trace peaks close to 0, with a positive shoulder). We plotted the methylation status of nDME^{CTD}-unique loci in wild-type endosperm to assess how they are demethylated by DME. This resulted in positive peaks for shorter (red trace) or longer (blue trace) TEs and intergenic sequences (green trace), showing that these nDME^{CTD}-unique loci are also demethylated by DME but not to a sufficient degree to reach the DMR cutoff. In contrast, most nDME^{CTD}-unique loci within coding sequences are not demethylated by DME (Fig. 4 *A*, orange trace). This indicates that genic sequences are the primary ectopic targets of nDME^{CTD}. This is also reflected by an increase in nDME^{CTD} DMR frequency (Fig. 4 *B*, red and orange traces) and a decrease in average CG methylation (*SI Appendix*, Fig. S5) within coding genes.

Gene body CG methylation, or gbM, is an evolutionarily conserved feature in mammals and angiosperms, but the origin and function of gbM has not been elucidated (3, 4). Approximately 15% (~5,000) of *Arabidopsis* genes contain gbM (31). In our endosperm methylomes, we found 2,202 and 3,213 genes associated with DME and nDME^{CTD} DMRs, respectively, which were largely mutually exclusive and thus constituted almost all of the genes with gbM (Fig. 4*C*). Among these, 2,260 genes were ectopically targeted by nDME^{CTD} (Fig. 4*C* and Dataset S1). Compared with DME-targeted coding genes, these nDME^{CTD}-unique genes have higher expression levels (Fig. 4*D*) and greater CG methylation (Fig. 4*E*). They include genes across most actively used cellular processes (*SI Appendix*, Table S6), consistent with the current theory that moderate gbM positively correlates with constitutively transcribed genes (3). Thus, nDME^{CTD} has a greater tendency than DME to target higher CG methylated coding sequences compared with lower methylated genes.

Evolutionary History of the DME/ROS1 Glycosylase Family. We show that the catalytic region of DME is able to demethylate DNA in vivo and also has targeting ability. We also demonstrate that the N terminus likely plays a role in fine-tuning DME targeting to heterochromatin and restricting it from gene bodies. To provide clues as to the evolutionary origin of these bipartite domains, we carried out comparative analyses across plant lineages. Using various DME homologs as query sequences, we revealed a diversity of N-terminal domains associated with the DME catalytic core across various clades (Fig. 5). These indicate that a shorter protein, comprising only the C terminus of *Arabidopsis* DME, may represent the ancestral form of the 5mC glycosylase found in all plant lineages. Variations of the N-terminal domains are found in land plants and charophytes (Streptophyta), which have a divergent circularly permuted CXXC domain between the FCL and RRMF domains. In contrast, 1 or more copies of the classical CXXC can be found in chlorophyte and stramenopile algae at distinct positions. Chlorophyte

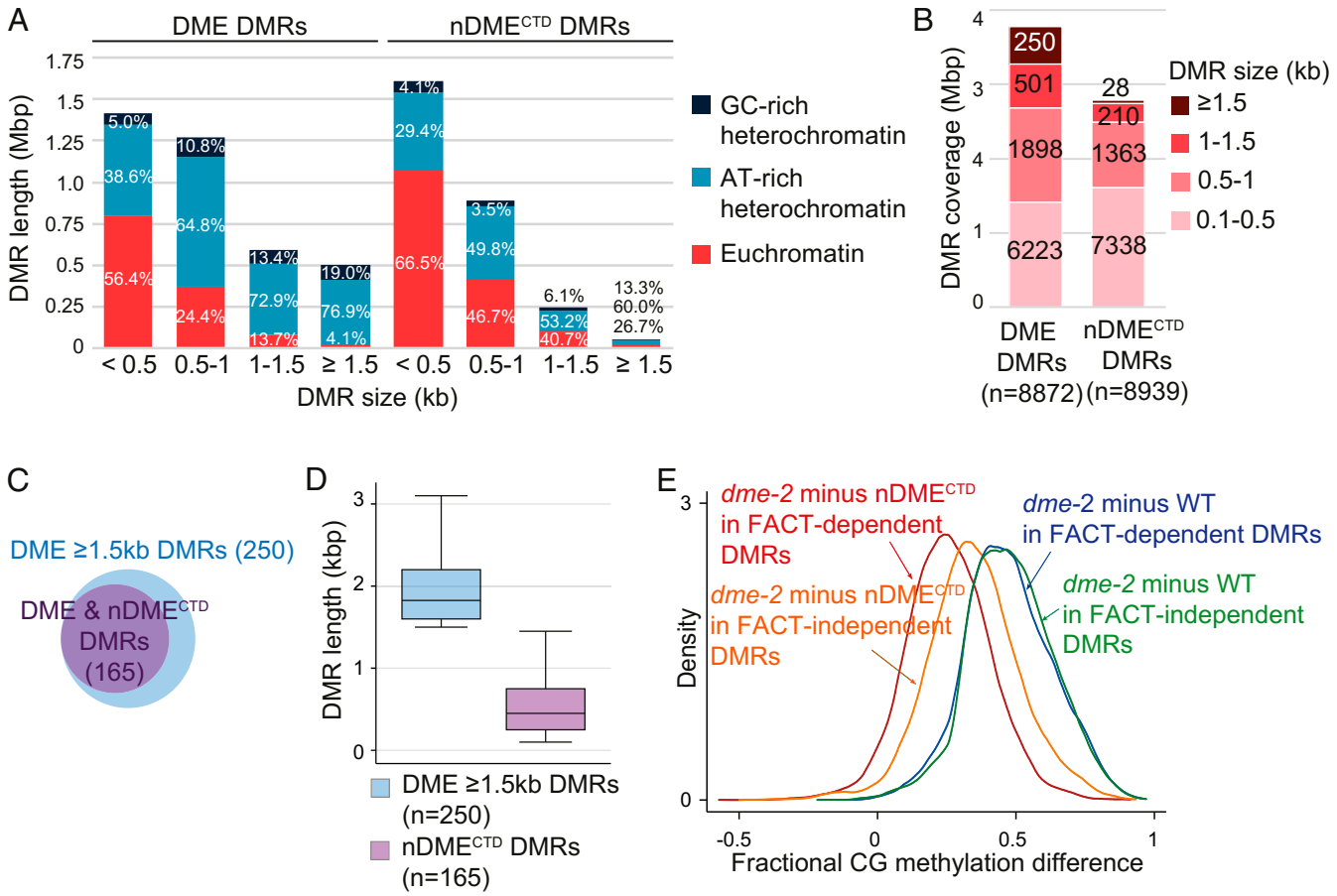

Fig. 3. DME and nDME^{CTD} DMRs. (*A*) Distribution of euchromatin and heterochromatin within each DMR length group. (*B*) DME and nDME^{CTD} DMRs grouped by size, with the total length that they cover shown. (*C* and *D*) The majority of the 250 longer DME DMRs overlap with the DMRs of nDME^{CTD}(*C*), but the nDME^{CTD} DMRs are shorter (*D*). (*E*) FACT dependency of the DME targets demethylated by DME (FACT-dependent, dark-green trace; FACT-independent, light-green trace) or by nDME^{CTD} (FACT-dependent, magenta trace; FACT-independent, orange trace).

and stramenopile homologs also have additional chromatin readers, such as Tudor and PHD; DNA-binding domains, such as the AT-hook; and the Hsp70-interacting DnaJ domains (27). These accessory domains suggest a mode of regulating DNA glycosylase activity according to methylation status (via CXXC) or chromatin states (via PHD and Tudor). The DemeN and basic stretch of the DME N-terminal region are restricted to the angiosperm lineage and appear to be a late acquisition during land plant evolution (Fig. 5). Thus, the acquisition of this region coincides with the origins of double fertilization in plants and the emergence of plant gene imprinting.

Discussion

DME regulates gene imprinting and influences transgenerational epigenetic inheritance in *Arabidopsis* (32). DME demethylates the central and vegetative gamete companion cell genomes at thousands of loci, but the mechanism of DME targeting remains elusive. This is due to the restriction of its expression to the ephemeral nuclei embedded within gametophytes, which largely prohibits biochemical interrogation by currently available tools. In contrast, genetic analysis coupled with endosperm transcriptome and methylome profiling has been instrumental in revealing DME's molecular function (9, 12–14, 23, 33). Here we used genetic complementation and endosperm DNA methylation profiling to show that the catalytic core of DME is sufficient to rescue the *dme* seed abortion phenotype and pollen germination defects (Fig. 1). We present evidence that nDME^{CTD} can demethylate most canonical DME target sites, implying that the catalytic region contains targeting information. We propose the DME protein has a bipartite structure (Fig. 6) and demonstrate a requirement for the N-terminal region in assisting heterochromatin demethylation, possibly via FACT.

Although *nDME^{CTD}* complements *dme*-associated developmental defects (Fig. 1*B* and *SI Appendix*, Tables S1 and S3), it does not fully rescue the *dme* endosperm DNA hypermethylation phenotype. Instead, we observed a reduced degree of demethylation by nDME^{CTD} in all the endogenous DME target loci, regardless of length (Fig. 2*A* and *SI Appendix*, Fig. S3*C*). To investigate the cause of this partial demethylation, we carried out data analyses to rule out technical differences in how experiments were performed. First, the nDME^{CTD} methylomes were generated from selfing Col transgenic lines, whereas the control wild-type and *dme-2* endosperm methylomes were derived from crosses of Col and L*er* parents (13). To assess the extent to which the difference between ColxL*er* and ColxCol F1 endosperm affects methylomes and/or how sample collection and preparation methods might influence the DNA methylation profile, we compared the methylation differences between wild-type (Colx*Ler*) and *nDME^{CTD}*-complemented (ColxCol) endosperm at DME target sites and non-DME target sites. The kernel density plot shows a general trend toward slight hypomethylation at non-DME target sites in *nDME^{CTD}*-complemented endosperm. In contrast, a more substantial hypermethylation at DME target sites in *nDME^{CTD}*-complemented endosperm compared with

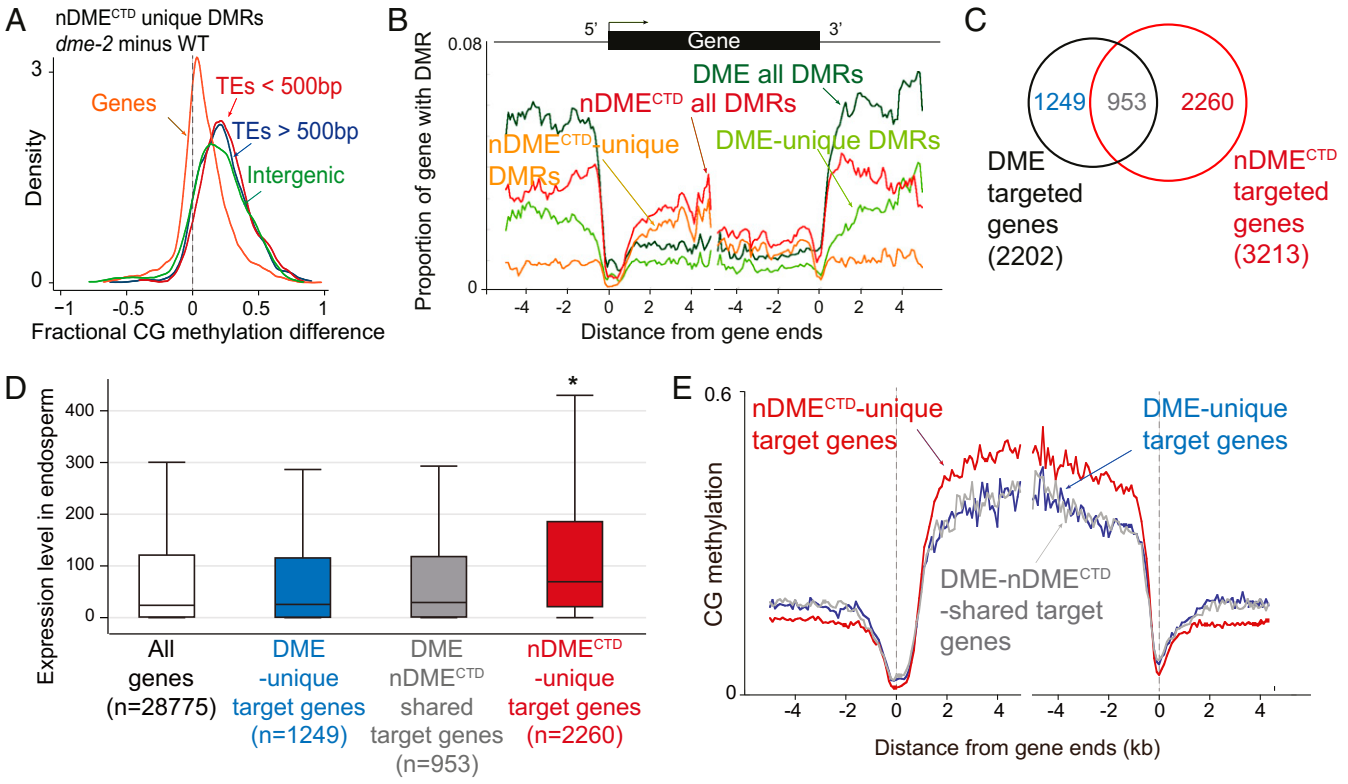

Fig. 4. nDME^{CTD} induces ectopic genic demethylation. (*A*) Kernel density plot of CG methylation differences between *dme-2* and wild-type endosperm for nDME^{CTD}-unique loci that reside in short (<500 bp, red trace) or longer (≥500 bp, blue trace) TEs, intergenic regions (green trace), or genic sequences (orange trace). (*B*) Distribution frequency of DMRs with respect to coding genes. Genes were aligned at the 5′ end or the 3′ end, and the proportion of genes with DMRs in each 100-bp interval is plotted. DMR distribution is shown with respect to all DME DMRs (dark-green trace), DME-unique DMRs (light-green trace), all nDME^{CTD} DMRs (red trace), and nDME^{CTD}-unique DMRs (orange trace). (*C*) Venn diagram showing the numbers of coding genes associated with DME and nDME^{CTD} DMRs. (*D*) Transcriptional scores (FPKM) in wild-type endosperm using expression data from ref. 33 for each group of genes indicated. Differences in expression level between nDME^{CTD}-unique target genes and all genes, DME-unique, or DME-nDME^{CTD}-shared target genes are significant (*$P < 0.0001$ for all comparisons, Wilcoxon rank-sum test). (*E*) Average CG methylation level of DME-unique target genes (blue trace), DME-nDME^{CTD}-shared target genes (gray trace), and nDME^{CTD}-unique target genes (red trace) in wild-type endosperm.

wild-type endosperm was detected (*SI Appendix*, Fig. S6*A*), indicating that the difference between ColxL*er* and ColxCol endosperm, or differing sample preparations, does not contribute to the hypermethylation of DME target loci in *nDME^{CTD}*-complemented endosperm.

We performed the following experiment to rule out the possibility that when propagating *dme-2* homozygous lines, loss of DME activity might cause epigenome alterations that render certain DME target loci no longer recognizable by nDME^{CTD}. Among the 3 independent *nDME^{CTD}*-complemented lines, 1 line (*nDME^{CTD}-3*) was propagated from a transformed *DME*/*dme-2* heterozygous plant in which the sporophyte was never *dme-2*/*dme-2* in the absence of the *nDME^{CTD}* transgene. Two other lines were generated by directly transforming *dme-2*/*dme-2* homozygous plants, with *dme-2* ovules derived from *dme-2*/*dme-2* megaspore mother cells before *nDME^{CTD}* complementation. Examination of the demethylation profiles of these 3 independent lines at DME canonical target loci revealed that the 3 lines had very similar demethylation profiles (*SI Appendix*, Fig. S6*B*), indicating that nDME^{CTD} partial demethylation is likely not a result of unexpected epigenome alternations induced by *dme-2*/*dme-2* plants.

The *nDME^{CTD}* transgene, although controlled by a native *DME* promoter and fully complemented *dme-2* seed abortion (Fig. 1 *B* and *C*), might lack critical regulatory elements needed to drive stable protein production to the levels comparable to the endogenous DME. Thus, an endosperm methylome complemented by a full-length DME cDNA construct within the otherwise similar T-DNA backbone as the *nDME^{CTD}* is needed to rule out any unforeseen artifacts introduced by the transgene. Throughout the course of this study, a full-length DME cDNA (*DME^{FL}*; ref. 15) was included side by side as a control for complementation assays and for methylation profiling. However, for reasons not completely understood, we observed that although it complemented *dme-2* seed abortion (3:1 ratio of viable to aborted F2 seeds, 1,518:556, $\chi^2 = 3.62$, $P = 0.057$; *SI Appendix*, Fig. S6*C* and Table S7) as reported previously (15, 34), the *DME^{FL}* consistently suffered from negative interference in the *dme-2* mutant background that resulted in very low demethylation activity in vivo, which most likely does not reflect the activity of the full-length DME protein (*SI Appendix*, Fig. S6*D*). To avoid confounding the interpretation, we excluded the *DME^{FL}* results and focused only on methylome comparisons between wild-type and *nDME^{CTD}*-complemented endosperm. Although we cannot completely rule out a negative effect of the *dme-2* genetic background on the *nDME^{CTD}* transgene, 2 factors suggest that this negative effect, if any, would be minimal. First, nDME^{CTD} generates roughly the same number of DMRs as the endogenous DME (Fig. 2*B*). Second, within the shared DMRs between nDME^{CTD} and DME, the degree of demethylation is quite comparable (Fig. 2*D* and *SI Appendix*, Fig. S7*A*). When directly comparing the difference between DME and nDME^{CTD} (DME minus nDME^{CTD}) in these completely overlapping DMRs that cover >1.2 million bases, the density plot peaks slightly to the negative side with a broader shoulder (*SI Appendix*, Fig. S7*B*),

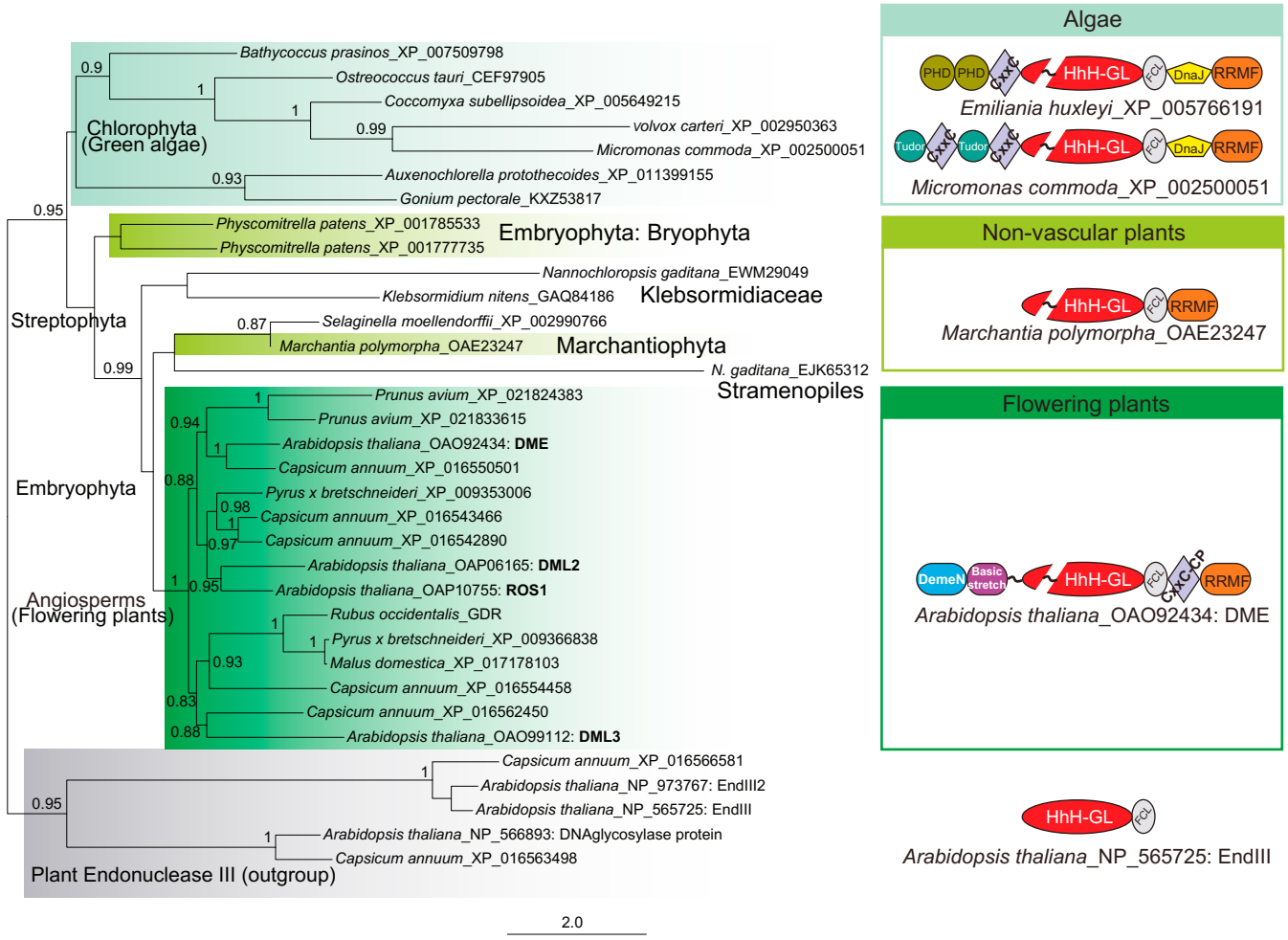

Fig. 5. Evolution of plant DME-like proteins. A phylogenetic tree was reconstructed using the PhyML program. Only nodes supporting values >0.80 from maximum likelihood bootstrap analyses are shown. The representative domain architectures of DME homologs in major plant clades are shown along the tree, demonstrating domain fusions during evolution. DemeN, N-terminal domain of DME-like proteins in angiosperms; DnaJ, DnaJ molecular chaperone homology domain (Pfam: PF00226); FCL, [Fe4S4] cluster loop motif (also called Iron-sulfur binding domain of endonuclease III; Pfam: PF10576); HhH-GL, HhH-GPD superfamily base excision DNA repair protein (Pfam: PF00730); PHD, PHD finger (Pfam: PF00628); RRMF, RNA recognition motif fold (Pfam: PF00076); Tudor, Tudor domain (Pfam: PF00567). The scale bar below the tree represents the number of substitutions per site.

indicating that $nDME^{CTD}$ is capable of demethylation to almost the DME level in these regions. Thus, we suspect that *$nDME^{CTD}$*-complemented endosperm methylome data can reasonably reflect the catalytic activity of the nuclear-localized DME^{CTD}. However, we also caution that in the absence of a proper full-length DME cDNA control, we cannot completely rule out that partial demethylation of DME^{CTD} might be caused by other factors.

Finally, it is also possible that the N-terminal region may assist the glycosylase by binding to DNA templates (via the AT hook-like motif) to promote demethylation, and that without it, DME^{CTD} has a reduced affinity to target DNA and exhibits lower demethylation activity. Previous studies of ROS1 support such a model, showing that the basic stretch/AT-hook region of ROS1 binds strongly to DNA templates in vitro in a non–sequence-specific manner, and that removal of the ROS1 basic stretch region impairs the sliding capacity of ROS1 on the DNA template (35), significantly reducing ROS1 5mC excision activity (25).

DME preferentially targets smaller euchromatic transposons that flank coding genes, and also targets gene-poor heterochromatin regions for demethylation (13). Since heterochromatin regions are compacted, demethylation in these regions requires substantial chromatin remodeling, including the temporary eviction of nucleosomes for DME to gain access to DNA. The FACT complex has been shown to be required for DME-mediated demethylation, primarily at heterochromatin targets (23), and we also noted that these sites have increased nucleosome occupancy (*SI Appendix*, Fig. S8). It is tempting to speculate that the DME N-terminal region is required to recruit factors such as FACT, and indeed we found that the overwhelming majority of the 250 longer DME DMRs (87%) that were not properly demethylated in the absence of the N-terminal region also require FACT activity for demethylation (Dataset S2). SPT16 has been shown to colocalize with DME in vivo (23), suggesting a direct or indirect interaction between DME and FACT.

$nDME^{CTD}$ also displayed a reduced capacity for demethylating FACT-independent loci. Thus, it is possible that the N-terminal region is needed to recruit other chromatin remodelers at FACT-independent targets, that is, if nucleosomes are natural barriers for DME demethylation in euchromatin as well as heterochromatin (*SI Appendix*, Fig. S8). We envision a working model (Fig. 6) in which the catalytic region directs DME to target sites, while the N-terminal region is required to interact with the local chromatin environment, stabilizing binding to the

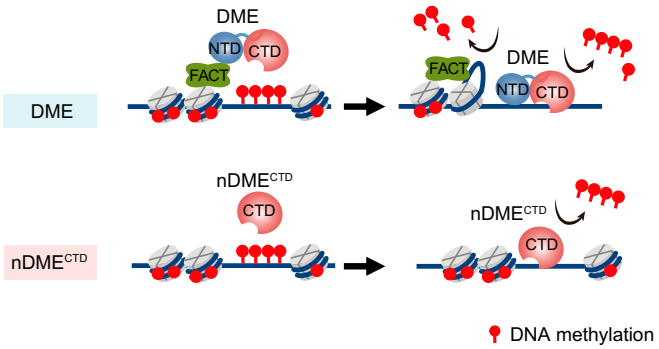

Fig. 6. A bipartite model for DME-mediated active demethylation. We propose a bipartite organization of DME in which the targeting and recruitment information is contained within the C-terminal catalytic core. In the absence of the N-terminal domain, processing of heterochromatin demethylation is significantly impeded, presumably by the chromatin structure. The N-terminal domain is required to recruit the FACT complex for the heterochromatic targets to overcome nucleosomal obstacles. The N-terminal conserved domains were acquired late during land plant evolution and are restricted to the angiosperm linage, suggesting a mode of demethylation regulation specific to angiosperm genomes.

chromosomal template and/or aiding demethylation of flanking sequences by remodeling nucleosomes.

gbM is evolutionarily conserved, and approximately 15% of *Arabidopsis* genes contain gbM (4). CG-methylated genes are often constitutively expressed housekeeping genes (3), raising the possibility that these genic methylated genes reside in open chromatin that is more accessible by nDME^{CTD} than by DME. It is also possible that DME is actively repelled by certain open chromatin histone marks, and such repulsion is missing in nDME^{CTD}. This scenario would be analogous to the mammalian de novo DNA methyltransferase DNMT3, where its binding to an allosteric activator, unmethylated histone H3, is strongly inhibited by H3K4 methylation (36). Equally probable is that additional factor(s) (e.g., methyl-binding proteins) might be associated with these higher CG-methylated genes (Fig. 4*E*) that restrict DME access.

Tracing the evolutionary history of DME-like genes (Fig. 5), we found that a bacterial version of the HhH-FCL pair underwent a horizontal gene transfer to the ancestor of plants, followed by a gene duplication. One copy was fused to an RRMF domain and further acquired an insert in the glycosylase domain, giving the ancestral form of DME in plants. This was likely then transferred to the stramenopiles from a secondary chlorophyte endosymbiont of this lineage. Finally, at the base of the streptophyte radiation, DME acquired a permuted CXXC, and later the DemeN domain and associated charged repeats were acquired in angiosperms, possibly to facilitate and ensure robust and thorough DNA demethylation. Thus, the adoption of a DME-based demethylation system for DNA base modification appears to have occurred early in the plant lineage. The presence of several accessory domains in addition to the conserved core suggests variation in the chromatin environment in specific lineages. For example, the presence of the DemeN and basic stretch/AT-hook motifs in angiosperms and the permuted CXXC domain in the Streptophyta lineage likely reflects adjustment to the unique methylation and chromatin environment of the larger Streptophyta and land plant genomes.

Our study shows that the catalytic core of DME was present in ancient plant ancestors and is alone capable of targeting and demethylation. The N-terminal domains, confined to flowering plant DME proteins, likely evolved to facilitate access to diverse chromatin states, in turn mediating gene imprinting and the transgenerational silencing of transposons (13).

Experimental Procedures

Detailed descriptions of the experimental methods are provided in *SI Appendix, Methods*. Sequencing data have been deposited in the Gene Expression Omnibus database (accession no. GSE130559).

Plant Materials and Seed Phenotype Analysis. Heterozygous *DME/dme-2* lines in the Col-*gl* background were subjected to *Agrobacterium*-mediated transformation. Seeds were sterilized with 30% bleach solution; plated on a 0.5× MS nutrient medium with 1.5% sucrose, 0.8% agar, and 40 μg/mL hygromycin; and stratified at 4 °C for 2 d. Germinated seedlings were transferred to soil and grown in a growth room under a 16-h light/8-h dark cycle at 23 °C. Siliques from T_1 transgenic plants were dissected at 14–16 d after self-pollination using a stereoscopic microscope (SteREO Discovery.V12; Carl Zeiss). The numbers of viable and aborted seeds in transgenic lines were statistically analyzed with the χ^2 test. The probabilities of deviation from a 1:1 or 3:1 segregation ratio for viable and aborted seeds were also calculated.

RNA Extraction, cDNA Synthesis, and qRT-PCR Analysis. Total RNA was extracted using TRIzol reagent (Invitrogen) and treated with TURBO DNase (Ambion) according to the manufacturers' instructions. For cDNA synthesis, 5 mg of total RNA was reverse-transcribed using SuperScript III reverse transcriptase and oligo(dT) primer (Invitrogen). cDNA was treated with RNase H (Invitrogen) at 37 °C for 20 min and then diluted 10-fold with H_2O. For each 15-μL qPCR reaction, 1 μL of diluted cDNA was used. qRT-PCR analyses were run on an Applied Biosystems 7500 Fast Real-Time PCR System using Roche FastStart Universal SYBR Green Master Mix. The qRT-PCR primers are listed in *SI Appendix*, Table S8. Ct values were normalized against *ACT2* (*At3g18780*) mRNA or *UBC* (*At5g25760*) mRNA. The abundance of mRNAs was expressed as relative to controls, with the control value set to 1. The error bars represent the SD of 4 biological replicates.

Protein Domain Analysis and Phylogenetic Inference. We used a domain-centric computational strategy to study DME and its related proteins. Specifically, we identified DME homologs using iterative profile searches with PSI-BLAST (37) from the protein nonredundant database at the National Center for Biotechnology Information. Multiple sequence alignments were built using PROMALS (38), followed by careful manual adjustments. Consensus secondary structures were predicted using the PSIPRED (39) JPred program (40). Conserved domains were further characterized based on comparisons with available domain models from Pfam (41) and sequence/structural features. PhyML (42) was used to determine the maximum likelihood tree using the Jones–Taylor–Thornton model for amino acids substitution with a discrete gamma model (4 categories with gamma shape parameter 1.096). The tree was rendered using MEGA Tree Explorer (43).

ACKNOWLEDGMENTS. We thank J.-Y. Lin (University of California, Los Angeles), P.-H. Hsieh (Joint Genome Institute), D. B. Lyons (University of California, Berkeley), and Y. Choi (Seoul National University) for suggestions and critical reading of the manuscript. This work is supported by the National Institute of Food and Agriculture Hatch Project 02413 (to T.-F.H.), NSF Grant MCB-1715115 (to T.-F.H. and W.X.), National Agricultural Genome Program Grant PJ013440 and Woo Jang-Choon Project Grant PJ009106 from the Rural Development Administration, Republic of Korea (to J.H.H.), NIH Grant R01-GM69415 (to R.L.F.), and the NIH Intramural Research Program (L.M.I. and L.A.).

1. J. A. Law, S. E. Jacobsen, Establishing, maintaining and modifying DNA methylation patterns in plants and animals. *Nat. Rev. Genet.* **11**, 204–220 (2010).
2. W. Reik, Stability and flexibility of epigenetic gene regulation in mammalian development. *Nature* **447**, 425–432 (2007).
3. D. Zilberman, An evolutionary case for functional gene body methylation in plants and animals. *Genome Biol.* **18**, 87 (2017).
4. A. J. Bewick, R. J. Schmitz, Gene body DNA methylation in plants. *Curr. Opin. Plant Biol.* **36**, 103–110 (2017).
5. B. P. Williams, M. Gehring, Stable transgenerational epigenetic inheritance requires a DNA methylation-sensing circuit. *Nat. Commun.* **8**, 2124 (2017).
6. O. Deniz, J. M. Frost, M. R. Branco, Regulation of transposable elements by DNA modifications. *Nat. Rev. Genet.* **20**, 417–431 (2019). Erratum in: *Nat. Rev. Genet.* **20**, 432 (2019).
7. M. A. Matzke, R. A. Mosher, RNA-directed DNA methylation: An epigenetic pathway of increasing complexity. *Nat. Rev. Genet.* **15**, 394–408 (2014).
8. T. F. Hsieh, Epigenetics: A tug of war for DNA methylation. *Nat. Plants* **2**, 16171 (2016).

9. M. Gehring *et al*., DEMETER DNA glycosylase establishes MEDEA polycomb gene self-imprinting by allele-specific demethylation. *Cell* **124**, 495–506 (2006).
10. F. Agius, A. Kapoor, J. K. Zhu, Role of the Arabidopsis DNA glycosylase/lyase ROS1 in active DNA demethylation. *Proc. Natl. Acad. Sci. U.S.A.* **103**, 11796–11801 (2006).
11. T. Morales-Ruiz *et al*., DEMETER and REPRESSOR OF SILENCING 1 encode 5-methylcytosine DNA glycosylases. *Proc. Natl. Acad. Sci. U.S.A.* **103**, 6853–6858 (2006).
12. M. Gehring, K. L. Bubb, S. Henikoff, Extensive demethylation of repetitive elements during seed development underlies gene imprinting. *Science* **324**, 1447–1451 (2009).
13. C. A. Ibarra *et al*., Active DNA demethylation in plant companion cells reinforces transposon methylation in gametes. *Science* **337**, 1360–1364 (2012).
14. T. F. Hsieh *et al*., Genome-wide demethylation of Arabidopsis endosperm. *Science* **324**, 1451–1454 (2009).
15. Y. Choi *et al*., DEMETER, a DNA glycosylase domain protein, is required for endosperm gene imprinting and seed viability in Arabidopsis. *Cell* **110**, 33–42 (2002).
16. J. Penterman *et al*., DNA demethylation in the Arabidopsis genome. *Proc. Natl. Acad. Sci. U.S.A.* **104**, 6752–6757 (2007).
17. R. Lister *et al*., Highly integrated single-base resolution maps of the Arabidopsis genome. *Cell* **133**, 395–397 (2008).
18. J. S. Park *et al*., Control of DEMETER DNA demethylase gene transcription in male and female gamete companion cells in Arabidopsis thaliana. *Proc. Natl. Acad. Sci. U.S.A.* **114**, 2078–2083 (2017).
19. V. K. Schoft *et al*., Function of the DEMETER DNA glycosylase in the Arabidopsis thaliana male gametophyte. *Proc. Natl. Acad. Sci. U.S.A.* **108**, 8042–8047 (2011).
20. M. Gehring, Genomic imprinting: Insights from plants. *Annu. Rev. Genet.* **47**, 187–208 (2013).
21. C. Köhler, P. Wolff, C. Spillane, Epigenetic mechanisms underlying genomic imprinting in plants. *Annu. Rev. Plant Biol.* **63**, 331–352 (2012).
22. J. H. Huh, M. J. Bauer, T.-F. Hsieh, R. L. Fischer, Cellular programming of plant gene imprinting. *Cell* **132**, 735–744 (2008).
23. J. M. Frost *et al*., FACT complex is required for DNA demethylation at heterochromatin during reproduction in Arabidopsis. *Proc. Natl. Acad. Sci. U.S.A.* **115**, E4720–E4729 (2018).
24. Y. Ikeda *et al*., HMG domain containing SSRP1 is required for DNA demethylation and genomic imprinting in Arabidopsis. *Dev. Cell* **21**, 589–596 (2011).
25. M. I. Ponferrada-Marín, M. I. Martínez-Macías, T. Morales-Ruiz, T. Roldán-Arjona, R. R. Ariza, Methylation-independent DNA binding modulates specificity of Repressor of Silencing 1 (ROS1) and facilitates demethylation in long substrates. *J. Biol. Chem.* **285**, 23032–23039 (2010).
26. Y. G. Mok *et al*., Domain structure of the DEMETER 5-methylcytosine DNA glycosylase. *Proc. Natl. Acad. Sci. U.S.A.* **107**, 19225–19230 (2010).
27. L. M. Iyer, S. Abhiman, L. Aravind, Natural history of eukaryotic DNA methylation systems. *Prog. Mol. Biol. Transl. Sci.* **101**, 25–104 (2011).
28. H. K. Long, N. P. Blackledge, R. J. Klose, ZF-CxxC domain-containing proteins, CpG islands and the chromatin connection. *Biochem. Soc. Trans.* **41**, 727–740 (2013).
29. A. Cléry, M. Blatter, F. H. Allain, RNA recognition motifs: Boring? Not quite. *Curr. Opin. Struct. Biol.* **18**, 290–298 (2008).
30. J. Sequeira-Mendes *et al*., The functional topography of the Arabidopsis genome is organized in a reduced number of linear motifs of chromatin states. *Plant Cell* **26**, 2351–2366 (2014).
31. A. J. Bewick *et al*., On the origin and evolutionary consequences of gene body DNA methylation. *Proc. Natl. Acad. Sci. U.S.A.* **113**, 9111–9116 (2016).
32. J. A. Rodrigues, D. Zilberman, Evolution and function of genomic imprinting in plants. *Genes Dev.* **29**, 2517–2531 (2015).
33. T. F. Hsieh *et al*., Regulation of imprinted gene expression in Arabidopsis endosperm. *Proc. Natl. Acad. Sci. U.S.A.* **108**, 1755–1762 (2011).
34. Y. Choi, J. J. Harada, R. B. Goldberg, R. L. Fischer, An invariant aspartic acid in the DNA glycosylase domain of DEMETER is necessary for transcriptional activation of the imprinted MEDEA gene. *Proc. Natl. Acad. Sci. U.S.A.* **101**, 7481–7486 (2004).
35. M. I. Ponferrada-Marín, T. Roldán-Arjona, R. R. Ariza, Demethylation initiated by ROS1 glycosylase involves random sliding along DNA. *Nucleic Acids Res.* **40**, 11554–11562 (2012).
36. S. K. Ooi *et al*., DNMT3L connects unmethylated lysine 4 of histone H3 to de novo methylation of DNA. *Nature* **448**, 714–717 (2007).
37. S. F. Altschul *et al*., Gapped BLAST and PSI-BLAST: A new generation of protein database search programs. *Nucleic Acids Res.* **25**, 3389–3402 (1997).
38. J. Pei, N. V. Grishin, PROMALS: Towards accurate multiple sequence alignments of distantly related proteins. *Bioinformatics* **23**, 802–808 (2007).
39. D. W. Buchan, F. Minneci, T. C. Nugent, K. Bryson, D. T. Jones, Scalable web services for the PSIPRED Protein Analysis Workbench. *Nucleic Acids Res.* **41**, W349–W357 (2013).
40. J. A. Cuff, M. E. Clamp, A. S. Siddiqui, M. Finlay, G. J. Barton, JPred: A consensus secondary structure prediction server. *Bioinformatics* **14**, 892–893 (1998).
41. R. D. Finn *et al*., The Pfam protein families database: Towards a more sustainable future. *Nucleic Acids Res.* **44**, D279–D285 (2016).
42. S. Guindon *et al*., New algorithms and methods to estimate maximum-likelihood phylogenies: Assessing the performance of PhyML 3.0. *Syst. Biol.* **59**, 307–321 (2010).
43. K. Tamura, J. Dudley, M. Nei, S. Kumar, MEGA4: Molecular Evolutionary Genetics Analysis (MEGA) software version 4.0. *Mol. Biol. Evol.* **24**, 1596–1599 (2007).

Supplementary Information for

The Catalytic Core of DEMETER Guides Active DNA Demethylation in Arabidopsis

Changqing Zhang, Yu-Hung Hung, Hyun Jung Rim, Dapeng Zhang, Jennifer M. Frost, Hosub Shin, Hosung Jang, Fang Liu, Wenyan Xiao, Lakshminarayan M. Iyer, L. Aravind, Xiang-Qian Zhang, Robert L. Fischer, Jin Hoe Huh, and Tzung-Fu Hsieh

Xiang-Qian Zhang, Robert L. Fischer, Jin Hoe Huh, and Tzung-Fu Hsieh
E-mail: aacrav@163.com, rfischer@berkeley.edu, huhjh@snu.ac.kr, or thsieh3@ncsu.edu

This PDF file includes:

Supplementary text
Fig. S1 to S8
Table S1 to S9
References for SI reference citation

Other supplementary materials for this manuscript including the followings:

Dataset S1
Dataset S2

Zhang el al., Supplemental Information

Supplementary Methods

Construction of transgenes used in this study.

A binary plasmid vector, pFGAMh, was modified to facilitate the generation of plasmid constructs using the Gibson assembly method. In brief, the pFGAMh vector backbone was derived from pFGC5941 (GenBank Accession: AY310901). In pFGAMh, the T-DNA region of pFGC5941 was replaced by a hygromycin resistance cassette as a plant selectable marker and a Gateway attR cassette (rfa, Invitrogen, Carlsbad CA, USA). The hygromycin resistant gene (HPTII) was driven by a mannopine synthase (MAS) promoter and terminated by a MAS terminator. The Gateway attR cassette was flanked with XhoI and XbaI unique restriction sites and followed by an octopine synthase (OCS) terminator.

The pDME: nDME^{CTD} plasmid comprises a linearized pFGAMh vector and three DNA fragments: a DME regulatory sequence (DMEpro), a bridge sequence, and the DME^{CTD} coding sequence (linker-DME^{CTD}). Vector plasmid pFGAMh was linearized by digesting with restriction enzymes XhoI and XbaI and removing Gateway attR cassette. The first fragment contains 2895 bp upstream of the DME.2 translation start codon ATG (DME regulatory sequence; DMEpro), which was PCR-amplified from Col-0 gDNA with primer pair VeDME/P3R. The second fragment was generated by annealing DNA oligos S40F and S40R that contains the Kozak consensus sequence (AACAATGGTG) and SV40 NLS (CCAAAGAAGAAGAGAAAGGTC). The third fragment was PCR-amplified from Col-0 cDNA with primer pair lnAGBF/CTDVeR. This fragment contains a 6-Alanine linker sequence and 3159 bp of C-terminal DME coding sequence (linker-DME^{CTD}, total 3174 bp). The linearized pFGAMh vector and the three DNA fragments were assembled using Gibson assembly (NEB) to generate pDME:nDME^{CTD}. Primer sequences are listed in Table S8.

An intermediate plasmid vector, DME-P3-attR-AGB, was generated by digesting plasmid pDME:SV40NLS::AGB with restriction enzymes AflII and NcoI to remove the Kozak consensus sequence, SV40 NLS, and 6 alanine linker. The linearized plasmid vector was then re-assembled with a 2800-bp fragment, which was produced through overlap PCR with 3 primer pairs, upAflII/P3attR, P3attF/attAGBR and attAGBF/dnNcoI, using Col-0 gDNA, attR cassette and Col-0 cDNA as templates, respectively. The resulting plasmid DME-P3-attR-AGB bears (1) the same 2895-bp regulatory sequence as the above constructs, (2) an attR cassette flanked by unique restrict sites XbaI and BglII, and (3) AGB coding sequence (3156 bp).

To generate pDME:DME^{FL}, plasmid DME-P3-attR-AGB was digested with XbaI and BglII to remove attR cassette. Overlap PCR with two primer pairs S1-5e/IN3R and IN3F/S1-5R amplified the N-terminal DME sequence (2985-bp) from Col-0 gDNA. The linearized vector and the 2985-bp DNA fragment were assembled using Gibson Assembly (NEB) to generate pDME:DME^{FL}, which carries the complete DME.2 coding sequence and intron 2 sequence (6075 bp) immediately downstream of the 2895-bp regulatory sequence with no additional sequences.

Isolation, propagation, and transformation of *dme-2*/*dme-2* homozygous lines.

We found *dme-2*/*dme-2* Col-*gl* plants can be easily obtained from *DME*/*dme-2* heterozygotes if seeds prior to desiccation were rescued on MS sucrose plates. This is consistent with the report that the *fis* endosperm cellularization defect and embryo arrest can be rescued by culturing the developing seeds in sucrose media because *fis* seeds have reduced hexose levels (1). Using this

method, we generated multiple homozygous lines, and we did not detect any difference between individuals in terms of normal seed rate or visible phenotype. The adult *dme-2*/*dme-2* plants are morphologically indistinguishable from wild-type Col-*gl* plants but produce ~0.1% viable mature seeds. These *dme-2*/*dme-2* plants are not due to genetic mutation or heritable aberrant epigenetic effects that escape the requirement of DME activity during gametogenesis because their subsequent progeny are phenotypically normal and produces same level (~0.1%) of normal seeds. For complementation assays in *dme-2*/*dme-2* homozygous plants, seeds were harvested from dipped T_0 plants. Transgenic plants were identified by germinating normal T_1 seeds on MS plates containing hygromycin. T1 plants carrying a single locus of complementing transgene in *dme-2*/*dme-2* transgenic plants produced siliques with 50% seed abortion rate. By contrast, when transforming *dme-2*/*dme-2* plants, a non-complementing transgene does not produce any transgenic plant.

Whole-Genome Bisulfite Sequencing and DNA Methylome Analysis.

Genomic DNA were isolated from hand dissected, 5-6 DAP *dme-2* endosperm that has been complemented by $nDME^{CTD}$ (*dme-2*/*dme-2*;$nDME^{CTD}$/$nDME^{CTD}$). Whole genome bisulfite sequencing libraries were constructed as described before with modifications (2, 3). Approximately 20-50 ng of purified genomic DNA was spiked with 0.5ng of unmethylated cl857 *Sam7* Lambda DNA (Promega, Madison, WI) and sheared to about 300bp using Covaris M220 (Covaris Inc., Woburn, Massachusetts) under the following settings: target BP, 300; peak incident power, 75 W; duty factor, 10%; cycles per burst, 200; treatment time, 90 second; sample volume 50μl. The sheared DNA was cleaned up and recovered by 1.2x AMPure XP beads then followed by end repaired and A-tailing (NEBNext Ultra II DNA Library Prep Kit for Illumina, NEB) before ligated to the NEBNext methylated multiplex adaptors (NEBNext Multiplex Oligos for Illumina, NEB) according to the manufacturer's instructions. Adaptor-ligated DNA was cleaned up with 1x AMPure XP beads. The purified adaptor-ligated DNA was spiked with 50ng of unmethylated cl857 *Sam7* Lambda DNA and subjected to one round of sodium bisulfite conversion using the EZ DNA Methylation-Lightning Kit (Zymo Research Corporation, Irvine, CA) as outlined in the manufacturer's instruction with 80 min of conversion time. Half of the bisulfite-converted DNA molecules was PCR amplified with the following condition: 2.5 U of ExTaq DNA polymerase (Takara), 5 ul of 10 x Extaq reaction buffer, 25 μM dNTPs, 1 ul of universal and index primers (10 uM) in 50 uL reaction. The thermocyling condition was as follows: 95 °C for 2 min and then 10 cycles each of 95 °C for 30 s, 65 °C for 30 s, and 72 °C for 60 s. The enriched libraries were purified twice with 0.8x (v/v) AMPure XP beads to remove adaptor dimers. High throughput sequencing was performed by Novogene Corporation (USA). Sequencing reads from three individual transgenic lines were used in the analysis (Table S9). We used the combined reads from the three independent lines for subsequent analyses since they were highly concordant, with Pearson correlation coefficients between combined independent lines, ranging between 0.92 and 0.94 (Table S4, see also whole genome average methylation plot analysis (Fig. S5)), and so that all comparisons were confined to the same cutoff criteria and comparable sequencing depth coverage.

Sequenced reads were mapped to the TAIR10 reference genomes and DNA methylation analyses were performed as previously described (2). Fractional CG methylation in 50-bp windows across the genome was compared between *dme-2*, wild-type (GSE38935), *and* $nDME^{CTD}$ -complemented endosperm. Windows with a fractional CG methylation difference of at least 0.3 in the endosperm comparison (Fisher's exact test p-value < 0.001) were merged to

generate larger differentially methylated regions (DMRs) if they occurred within 300 bp. DMRs were retained for further analysis if the fractional CG methylation across the merged DMR was 0.3 greater in *dme* endosperm than in wild-type or in *nDME*^{CTD} -complemented endosperm (Fisher's exact test p-value < 10^{-10}), and if the DMR is at least 100-bp long. The merged DMR list is in the supplemental Dataset S2. The *dme* and wild-type endosperm data used in this study were derived from crossed between Col (female parent) and L*er* (male parent) (GSE38935). To avoid potential ecotype-specific methylation difference, L*er* hyper-DMRs relative to Col-0 endosperms (GSE52814) were identified using the same criteria as described above and excluded from further analyses. The DMR Venn diagrams are made based on the number of the merged DMRs.

The *ssrp1*/+ endosperm sequencing reads (4), (GSE10500) were mapped to the TAIR10 reference genome. We compared ssrp1/+ and wild-type endosperm (GSE38935) to identify SSRP1 DMRs using the method described above. DME DMRs that intersect with SSRP1 DMRs (using BEDTools intersect function (5)) were determined as FACT-dependent DME DMRs, and the ones that do not intersect with SSRP1 DMRs were determined as FACT-independent DME DMRs. For further analysis of FACT-dependent loci, we only focus on the DME DMR windows that overlap with SSRP1 DMRs.

To investigate the distribution of DMRs along genes, all TAIR-annotated genes were aligned at the 5' end or the 3' ends. The proportion of genes with specific DMRs in each 100-bp interval is plotted (Fig. 4B).

Genomic coordinates of chromatin states were from (6), converted to 50 bp windows and aligned with *dme-2*, wild-type and *nDME*^{CTD} methylomes. Each 50 bp windows of wild-type DME and *nDME*^{CTD} DMRs was assigned a chromatin state accordingly.

Methylation average metaplots of Genes and TEs (Fig. S5) were performed as described previously (2).

The coordinates of the well-positioned (group 1) nucleosomes in wild-type rosette leaf was retrieved from (7). The number of well-positioned nucleosomes that intersect with FACT-dependent or -independent DME DMRs (using BEDTools intersect function (5)) was divided by the length of each DMR. The number of nucleosomes per 100-bp DMR was presented in the boxplot.

Supplementary Figures

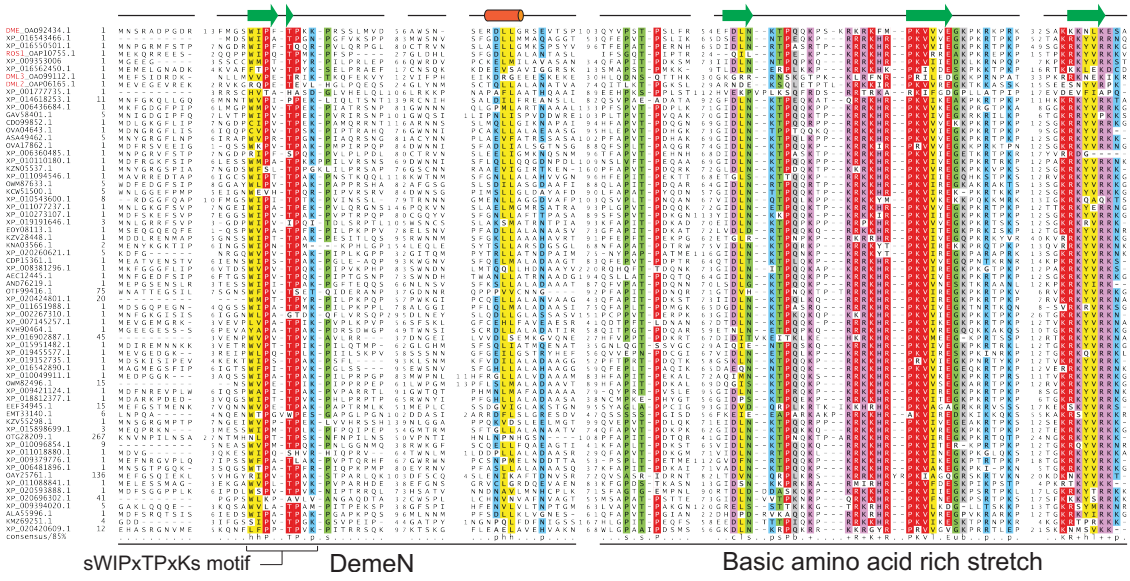

Fig. S1. Alignment of angiosperm DME-like proteins showing the conserved DemeN domain and basic stretch region. Bioinformatic analysis using available DME-like sequences identified a ~120-amino-acid-long conserved region at the very N-terminus of DME-like proteins in angiosperms. This sequence is characterized by a highly conserved sWIPxTPxKs motif that might function in protein-protein interactions. Further toward the C-terminus is a stretch of basic amino acids that serves as a nuclear localization signal. This sequence consists of direct repeats reminiscent of the AT-hook motifs that may bind DNA. Numbers flanking each sequence represent amino acid residue positions. Numbers between alignment blocks reflect residue gaps not shown in the alignment.

Fig. S2 Genome browser snapshots of CG DNA methylation at selected imprinted gene loci. Top two tracks are coding genes (magenta) and TEs (orange) with Tair10 chromosome coordinates. The bottom five tracks represent fractional CG methylation levels for different genotypes: black trace, *dme-2* endosperm; dark green trace, WT endosperm; dark blue trace, *nDME*^{CTD}-complemented endosperm; light green trace, WT endosperm subtracted from *dme-2* mutant endosperm; light purple trace, *nDME*^{CTD}-complemented endosperm subtracted from *dme-2* endosperm. *dme*-induced CG hypermethylation at selected maternally expressed (*FIS2* and *SDC*) and paternally expressed (*SUVH7*, *YUC10, and PHE1*) imprinted genes is rescued in *nDME*^{CTD}-complemented endosperm.

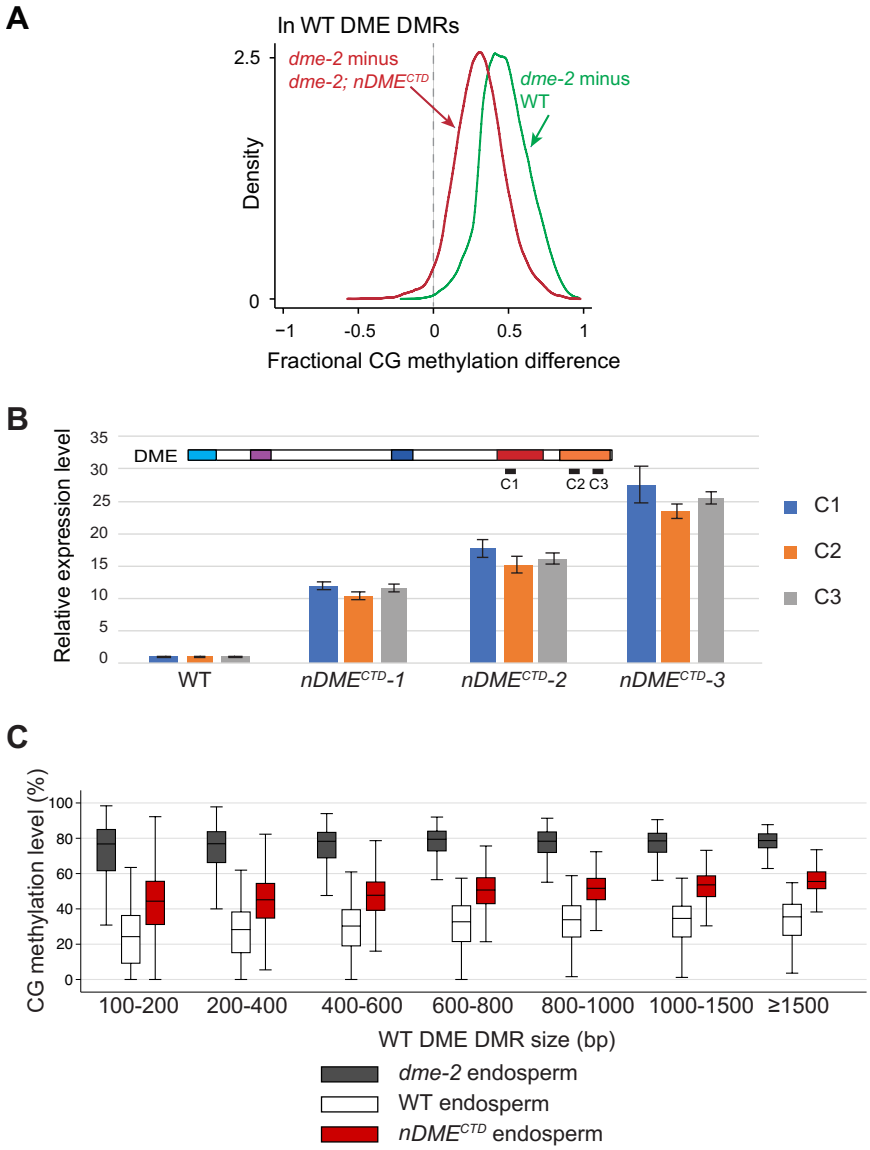

Fig. S3. (A) Kernel density plot of CG methylation differences between *dme* and *nDME*^{CTD}-complemented endosperm, for loci demethylated by DME. Green trace shows these DME target sites are hypermethylated in *dme* endosperm. Red trace shows these same DME target sites are partially demethylated by nDME^{CTD}. (B) qRT-PCR of *nDME*^{CTD} expression levels in the three independent nDME^{CTD}-complemented lines used in this study compared to that of the endogenous DME. (C) Boxplot of CG methylation levels within canonical DME target sites grouped by DMR length, in *dme-2* mutant (black), wild-type (white), or *nDME*^{CTD}-complemented (red) endosperm.

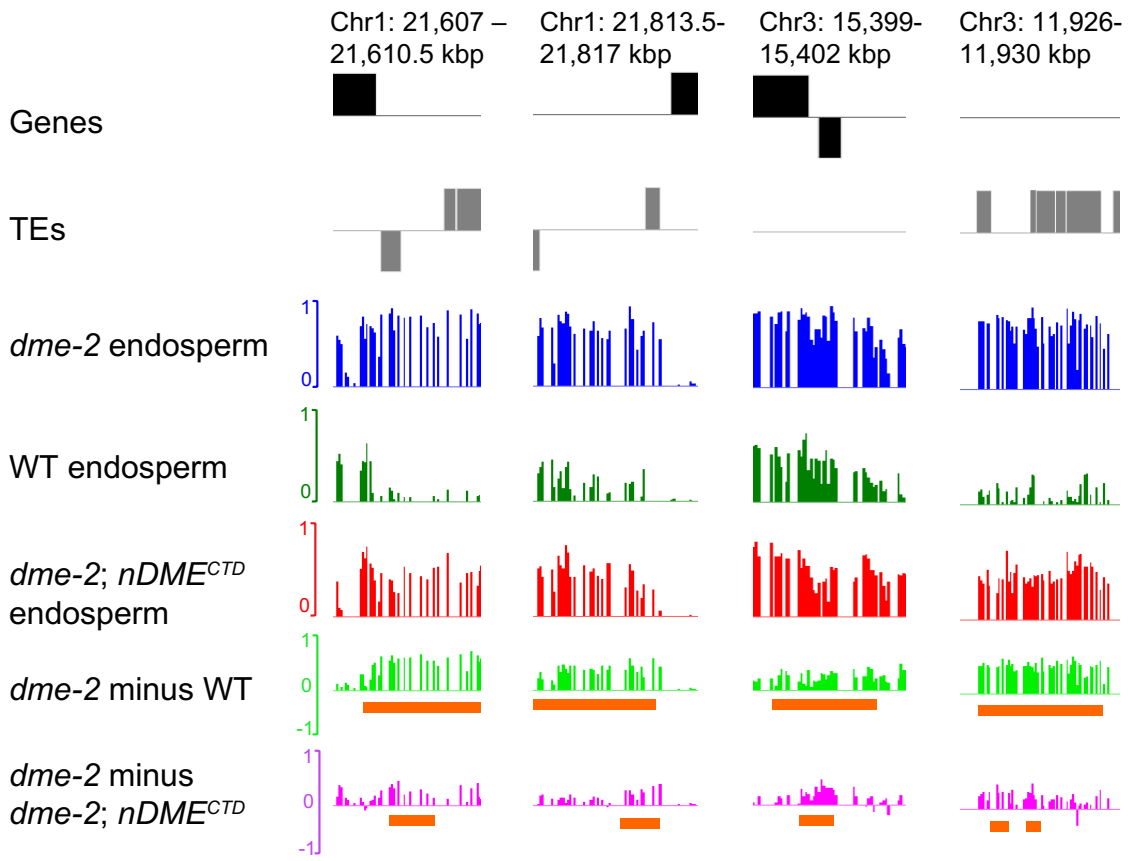

Fig. S4. Genome Browser snapshots of long wild-type DME DMRs. Tracks are as labeled. The DMR regions are indicated as horizontal bars (bottom two tracks) according to their length in each sample.

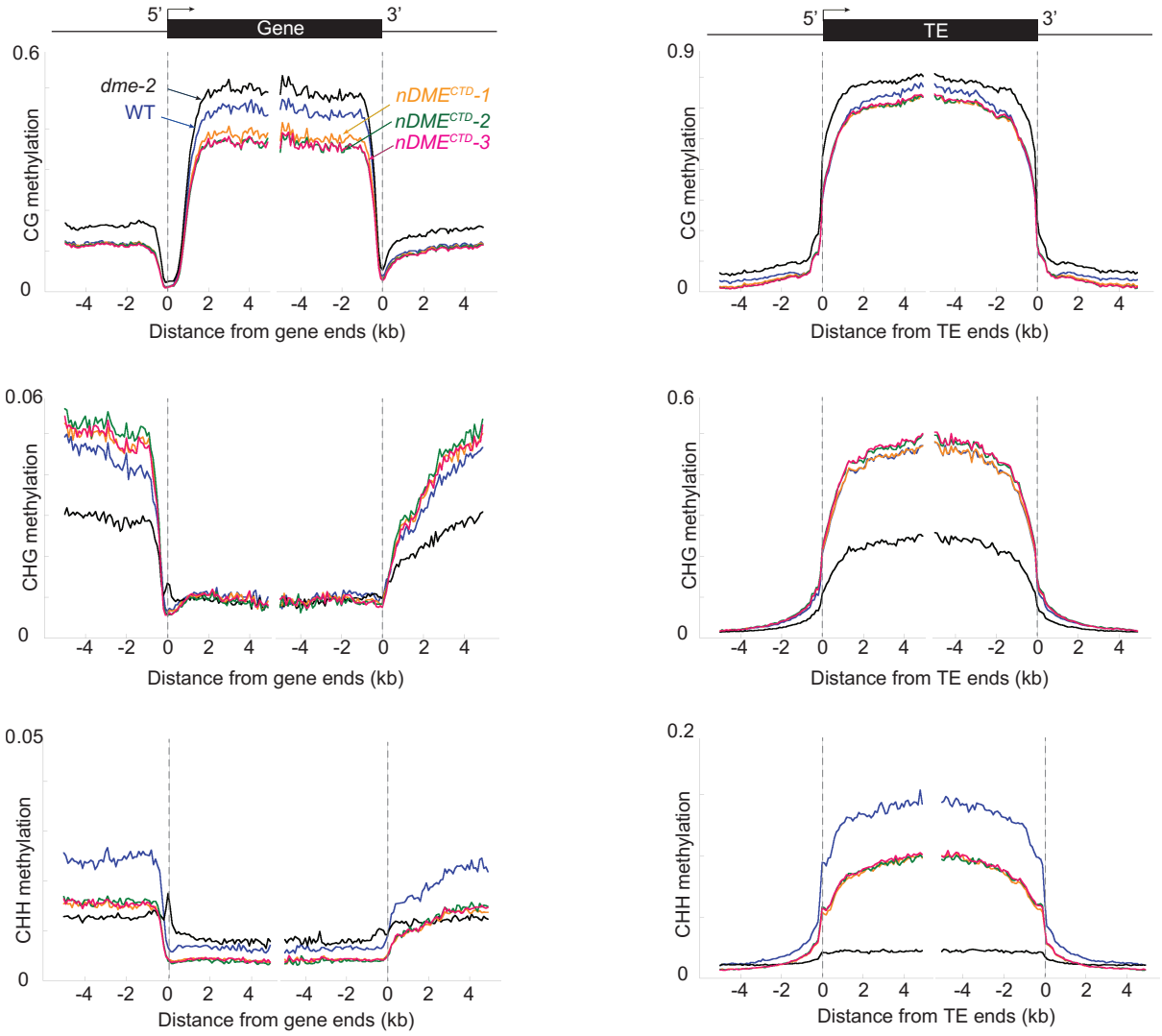

Fig. S5. Whole genome CG, CHG, CHH methylation average plots of three independent nDME^{CTD}-complemented lines, *dme-2* mutant, and wild-type endosperm. Average CG, CHG, CHH methylation in Genes (left panels) or TEs (right panels) of endosperm methylation data used in this study. Wildtype (WT) and *dme-2* endosperm data were from (2). Three nDME^{CTD}-complemented endosperm methylation profiles were as indicated. Endosperm were dissected from complemented lines from bent-cotyledon stage seeds.

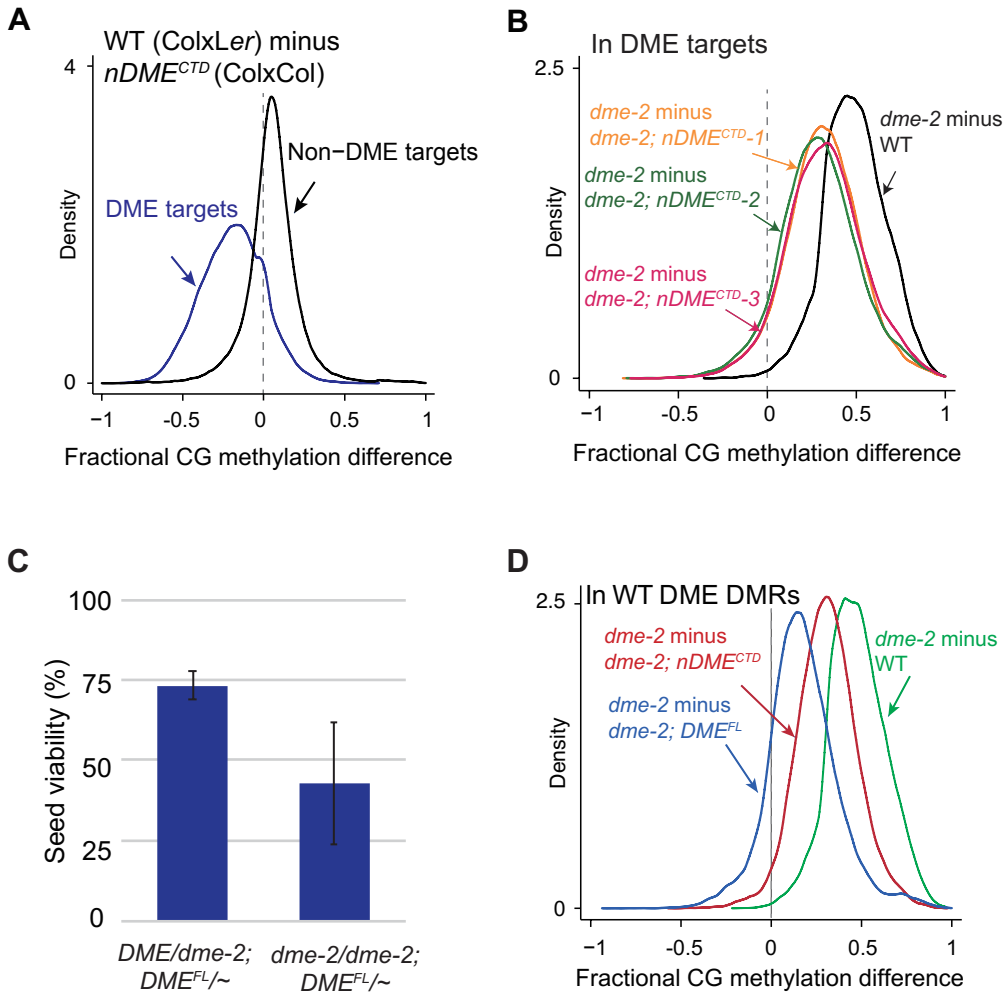

Fig. S6. Technical caveats associated with this study do not directly contribute to the observed partial DME^{CTD} demethylation activity. (A) Kernel density plot of CG methylation differences between wildtype (ColxLer) and *nDME*^{CTD}-complemented (ColxCol) endosperm, for loci targeted (blue trace) or not targeted by DME (black trace). (B) Kernel density plot of CG methylation differences between *dme-2* mutant endosperm and wildtype (black trace) and three individual lines of *nDME*^{CTD}-complemented endosperm in DME targets. (C) The percentages of viable seeds in *DME*/*dme-2* or in *dme-2*/*dme-2* plants that were complemented by *DME*^{FL} transgene. Error bars represent standard deviations. (D) Kernel density plot of CG methylation differences between *dme-2* and wildtype (green trace), *nDME*^{CTD}- (red trace), and *DME*^{FL}- (blue trace) complemented endosperm, for loci demethylated by DME.

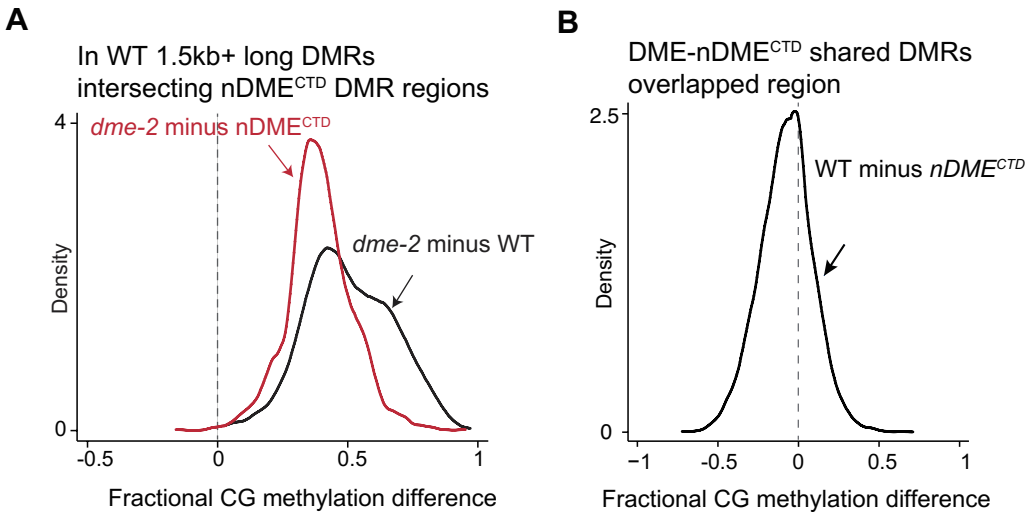

Fig. S7. (A) Kernel density plots of CG methylation differences between *dme-2* and nDME^{CTD}-complemented endosperm (red trace) or CG methylation differences between *dme-2* and WT endosperm (black trace), within the DME DMRs that are longer than 1.5kb that overlap with nDME^{CTD} DMRs. (B) Kernel density plot of CG methylation difference between WT and nDME^{CTD}-complemented endosperm within the DME-nDME^{CTD} shared DMRs that completely overlap. The overlap DMRs covers over 1.2 million bases.

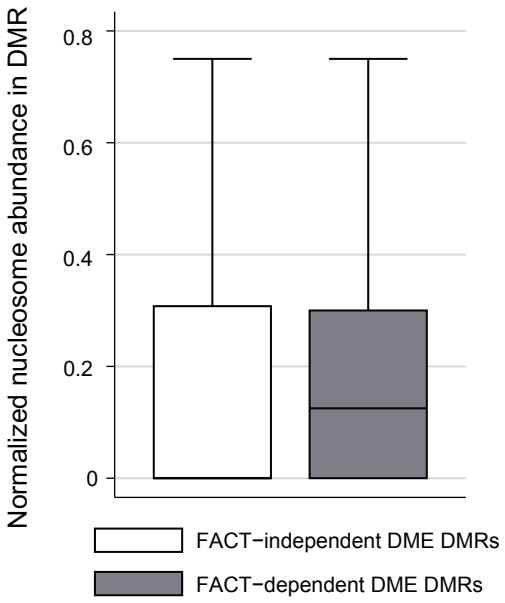

Fig. S8. Boxplot of relative nucleosome abundance in FACT-independent or -dependent DME DMRs, using genome coordinates of the most well-positioned nucleosomes in wild-type rosette leaves (7) that overlap with DME DMRs. Number of nucleosomes per 100-bp DMR is plotted

Supplementary Tables

Table S1. Seed abortion ratio of *dme-2* complemented by *nDME^{CTD}*

Genotype	No. of total seeds*	No. of viable seeds	Proportion of viable seeds (%)	*p* for 1:1†	*p* for 3:1†
DME/dme-2; pDME:nDME^{CTD}-2	347	287	83	3.7E-34	9.1E-04
DME/dme-2; pDME:nDME^{CTD}-1	444	372	84	5.4E-46	1.9E-05
DME/dme-2; pDME:nDME^{CTD}-3	171	119	70	3.0E-07	0.10
DME/dme-2; pDME:nDME^{CTD}-4	124	80	65	1.2E-03	0.01
DME/dme-2; pDME:nDME^{CTD}-45	282	213	76	9.9E-18	0.84
DME/dme-2; pDME:nDME^{CTD}-5	363	221	61	3.4E-05	5.2E-10
dme-2/dme-2; pDME:nDME^{CTD}-6	221	166	75	8.2E-14	0.97
dme-2/dme-2; pDME:nDME^{CTD}-8	284	206	73	3.1E-14	0.34
dme-2/dme-2; pDME:nDME^{CTD}-4	221	155	70	2.1E-09	0.09
dme-2/dme-2; pDME:nDME^{CTD}-11	413	269	65	7.7E-10	3.6E-06
dme-2/dme-2; pDME:nDME^{CTD}-3	351	206	59	1.1E-03	1.7E-12
dme-2/dme-2; pDME:nDME^{CTD}-16	229	131	57	0.03	5.0E-10
dme-2/dme-2; pDME:nDME^{CTD}15	413	208	50	0.88	6.4E-31
dme-2/dme-2; pDME:nDME^{CTD}-1	298	150	50	0.91	8.1E-23
dme-2/dme-2; pDME:nDME^{CTD}-10	300	151	50	0.91	5.8E-23
dme-2/dme-2; pDME:nDME^{CTD}-13	387	186	48	0.44	1.9E-34
dme-2/dme-2; pDME:nDME^{CTD}-12	223	83	37	1.3E-04	8.3E-39

* Total number of viable and aborted seed counted.

† Probability that the deviation from the indicated segregation ratio of viable: aborted seeds is due to chance.

Table S2. Reduced paternal *dme* allele transmission in the Col-*gl* ecotype

Genotype	Ecotype	*DME/dme-2* *	*DME/DME* *	*dme-2* (%) §	*p* †
DME/dme-2 self-pollination, plant 1	Col-*gl*	78	190	29	7.8E-12
DME/dme-2 self-pollination, plant 2	Col-*gl*	62	172	26	6.4E-13
DME/dme-2 self-pollination, plant 3	Col-*gl*	72	145	33	7.2E-7
DME/dme-2 self-pollination, plant 4	Col-*gl*	51	201	20	3.4E-21

* Number of F1 seed with indicated genotype.

§ *dme-2* allele transmission rate.

† Probability that that the deviation from the indicated segregation ration (1:1 inheritance of paternal genome with or without *dme-2* in the F1 generation) is due to chance.

Table S3. Complementation of *dme* allele pollen transmission by nDME^{CTD}

Maternal parent	Paternal parent	Paternal parent normal seed (%)	*DME/dme-2* *	*DME/dme-2*; *T* *	*T* (%) §	*p* †
Col-0	*dme-2/dme-2*; *nDME^{CTD}* Line 10	50	32	62	66	2.0E-3
Col-0	*dme-2/dme-2*; *nDME^{CTD}* Line 11	65	3	50	94.3	1.1E-10
Col-0	*dme-2/dme-2*; *nDME^{CTD}* Line 12	37	8	34	81	6.0E-5
Col-0	*dme-2/dme-2*; *nDME^{CTD}* Line 15	50	9	44	83	1.5E-6

* Number of F1 seed with indicated genotype. *T*, *nDME^{CTD}* transgene.

§ *T*, *nDME^{CTD}* transgene transmission rate.

† Probability that that the deviation from the indicated segregation ration (1:1 inheritance of paternal genome with or without *nDME^{CTD}* transgene in the F1 generation) is due to chance.

Table S4. Whole genome endosperm BS-seq data correlation between three independent complementation lines

Pearson correlation coefficient	*nDME*^{CTD}*-1* endosperm CG	*nDME*^{CTD}*-2* endosperm CG	*nDME*^{CTD}*-3* endosperm CG
nDME^{CTD}*-1* endosperm CG	1		
nDME^{CTD}*-2* endosperm CG	0.9423	1	
nDME^{CTD}*-3* endosperm CG	0.9317	0.9331	1

Table S5. Whole genome endosperm BS-seq data correlation between the three data sets used in this study excluding canonical DME target sites

Pearson correlation coefficient	*dme-2* endosperm CG	WT endosperm CG	*nDME*^{CTD} endosperm CG
dme-2 endosperm CG	1		
WT endosperm CG	0.9348	1	
nDME^{CTD} endosperm CG	0.9434	0.9244	1

Table S6. Gene enrichment analysis of *nDME^{CTD}*-unique target genes

GO Function	Total gene	*nDME^{CTD}*-unique target gene	Expected	Fold Enrichment	FDR (<0.05)
Biological Process					
gluconeogenesis (GO:0006094)	17	6	1	4.38	2.62E-02
regulation of gene expression, epigenetic (GO:0040029)	45	12	4	3.31	4.78E-03
DNA replication (GO:0006260)	129	25	10	2.41	1.89E-03
tRNA metabolic process (GO:0006399)	143	26	12	2.26	3.44E-03
RNA splicing, via transesterification reactions (GO:0000375)	202	36	16	2.21	4.09E-04
nuclear transport (GO:0051169)	119	21	10	2.19	9.86E-03
phospholipid metabolic process (GO:0006644)	110	19	9	2.14	1.89E-02
mRNA processing (GO:0006397)	310	52	25	2.08	7.04E-05
mRNA splicing, via spliceosome (GO:0000398)	224	37	18	2.05	1.39E-03
DNA repair (GO:0006281)	189	31	15	2.04	3.78E-03
DNA metabolic process (GO:0006259)	351	57	28	2.02	4.64E-05
protein transport (GO:0015031)	600	97	48	2.01	4.30E-08
intracellular protein transport (GO:0006886)	568	90	46	1.97	4.52E-07
phosphate-containing compound metabolic process (GO:0006796)	1688	259	136	1.9	4.34E-19
vesicle-mediated transport (GO:0016192)	520	78	42	1.86	1.54E-05
transcription from RNA polymerase II promoter (GO:0006366)	427	63	34	1.83	2.23E-04
cellular amino acid biosynthetic process (GO:0008652)	185	27	15	1.81	2.66E-02
nucleobase-containing compound metabolic process (GO:0006139)	2727	397	220	1.81	4.23E-26
protein localization (GO:0008104)	474	68	38	1.78	2.06E-04
cell cycle (GO:0007049)	532	76	43	1.77	1.04E-04
regulation of nucleobase-containing compound metabolic process (GO:0019219)	409	58	33	1.76	9.26E-04
RNA metabolic process (GO:0016070)	1603	227	129	1.76	3.94E-13
catabolic process (GO:0009056)	1290	176	104	1.69	5.58E-09
transcription, DNA-dependent (GO:0006351)	753	99	61	1.63	1.05E-04
transport (GO:0006810)	1441	187	116	1.61	4.46E-08
cellular protein modification process (GO:0006464)	783	99	63	1.57	4.09E-04
cellular component organization (GO:0016043)	1359	169	110	1.54	2.87E-06
localization (GO:0051179)	1580	194	127	1.52	8.15E-07
nitrogen compound metabolic process (GO:0006807)	2924	359	236	1.52	5.08E-13
cellular component organization or biogenesis (GO:0071840)	1640	198	132	1.5	1.62E-06
primary metabolic process (GO:0044238)	5340	631	430	1.47	3.18E-21
metabolic process (GO:0008152)	6924	811	558	1.45	9.32E-28
organelle organization (GO:0006996)	938	108	76	1.43	3.71E-03
cellular process (GO:0009987)	6866	780	553	1.41	4.33E-23
regulation of biological process (GO:0050789)	1302	144	105	1.37	2.59E-03
biological regulation (GO:0065007)	1526	164	123	1.33	3.16E-03
response to stimulus (GO:0050896)	1690	178	136	1.31	3.73E-03
protein metabolic process (GO:0019538)	1751	181	141	1.28	6.73E-03
biosynthetic process (GO:0009058)	2090	206	168	1.22	2.36E-02

Table S6. Continued.

Molecular Function					
lipid transporter activity (GO:0005319)	20	7	1.61	4.34	1.95E-02
enzyme activator activity (GO:0008047)	46	14	3.71	3.78	1.26E-03
nucleotidyltransferase activity (GO:0016779)	128	30	10.31	2.91	3.60E-05
DNA-directed RNA polymerase activity (GO:0003899)	60	14	4.83	2.9	8.04E-03
helicase activity (GO:0004386)	87	19	7.01	2.71	2.72E-03
DNA helicase activity (GO:0003678)	52	11	4.19	2.63	3.38E-02
microtubule motor activity (GO:0003777)	75	15	6.04	2.48	2.21E-02
anion channel activity (GO:0005253)	77	14	6.2	2.26	4.16E-02
translation regulator activity (GO:0045182)	105	19	8.46	2.25	1.93E-02
motor activity (GO:0003774)	94	17	7.57	2.24	2.98E-02
hydrogen ion transmembrane transporter activity (GO:0015078)	102	18	8.22	2.19	2.55E-02
pyrophosphatase activity (GO:0016462)	609	107	49.07	2.18	2.15E-10
GTPase activity (GO:0003924)	194	34	15.63	2.18	1.15E-03
ion channel activity (GO:0005216)	93	16	7.49	2.14	4.40E-02
mRNA binding (GO:0003729)	177	28	14.26	1.96	1.33E-02
nucleotide binding (GO:0000166)	141	22	11.36	1.94	3.49E-02
kinase activity (GO:0016301)	724	111	58.34	1.9	7.19E-08
receptor activity (GO:0004872)	361	54	29.09	1.86	8.57E-04
transmembrane receptor protein serine/threonine kinase activity (GO:0004675)	334	49	26.91	1.82	2.47E-03
signal transducer activity (GO:0004871)	305	44	24.58	1.79	5.60E-03
protein kinase activity (GO:0004672)	508	71	40.93	1.73	5.69E-04
transferase activity (GO:0016740)	1902	252	153.26	1.64	1.68E-11
RNA binding (GO:0003723)	739	86	59.55	1.44	1.16E-02
hydrolase activity (GO:0016787)	2086	238	168.08	1.42	8.75E-06
binding (GO:0005488)	3418	383	275.41	1.39	7.64E-09
nucleic acid binding (GO:0003676)	1759	195	141.73	1.38	4.22E-04
catalytic activity (GO:0003824)	5737	635	462.26	1.37	7.30E-15
protein binding (GO:0005515)	1594	175	128.44	1.36	1.17E-03
transporter activity (GO:0005215)	996	108	80.25	1.35	2.50E-02

Table S7 Seed abortion ratio of *dme-2* complemented by *DME*^{FL}.

Genotype	No. of total seeds*	No. of viable seeds	Proportion of viable seeds (%)	*p* for 1:1†	*p* for 3:1†
DME/dme-2; pDME:DME^{FL}*-50*	187	146	78	1.6E-14	0.33
DME/dme-2; pDME:DME^{FL}*-49*	402	312	78	1.7E-28	0.23
DME/dme-2; pDME:DME^{FL}*-33*	189	142	75	4.8E-12	0.97
DME/dme-2; pDME:DME^{FL}*-25*	340	254	75	8.2E-20	0.90
DME/dme-2; pDME:DME^{FL}*-39*	309	227	73	1.6E-16	0.53
DME/dme-2; pDME:DME^{FL}*-20*	350	241	69	1.7E-12	0.01
DME/dme-2; pDME:DME^{FL}*-7*	297	196	66	3.5E-08	3.4E-04
dme-2/dme-2; pDME:DME^{FL}*-1*	164	121	74	1.1E-09	0.72
dme-2/dme-2; pDME:DME^{FL}*-13*	128	76	59	3.4E-02	4.5E-05
dme-2/dme-2; pDME:DME^{FL}*-7*	171	95	56	0.15	4.3E-09
dme-2/dme-2; pDME:DME^{FL}*-9*	188	98	52	0.56	4.4E-13
dme-2/dme-2; pDME:DME^{FL}*-5*	489	250	51	0.62	3.4E-34
dme-2/dme-2; pDME:DME^{FL}*-16*	191	88	46	0.28	2.6E-20
dme-2/dme-2; pDME:DME^{FL}*-6*	504	223	44	0.01	3.1E-57
dme-2/dme-2; pDME:DME^{FL}*-15*	188	67	36	8.2E-05	1.2E-35
dme-2/dme-2; pDME:DME^{FL}*-2*	465	129	28	8.0E-22	1.8E-122
dme-2/dme-2; pDME:DME^{FL}*-3*	421	82	19	5.4E-36	1.5E-152
dme-2/dme-2; pDME:DME^{FL}*-16*	302	30	10	4.4E-44	2.6E-150

* Total number of viable and aborted seed counted.

† Probability that the deviation from the indicated segregation ratio of viable: aborted seeds is due to chance.

Table S8. Primer list

Primers used for plasmid construction:	
VeDME	AGTGGAGACGGACGTCCTGACGCCCTCAAAAATGTCTTCTTAGGATCACAAAATC
P3R	CACCATTGTTAACACACTTGATGAATCACTCCCCCTTC
lnAGBF	GCTGCCGCAGCGGCTGCCTACAAAGGAGATGGTGCACTTGTT
CTDVeR	AGGACTCTAGGGACTAGTCCCGGGTTTAGGTTTTGTTGTTCTTCAATTTGCTCGCAG
ATGF	TTCATCAAGTGTGTTAACAATGGTGGCTGCCGCAGCGGCTGCCTACAAAG
ATGR	CTTTGTAGGCAGCCGCTGCGGCAGCCACCATTGTTAACACACTTGATGAA
S40F	TTCATCAAGTGTGTTAACAATGGTGCCAAAGAAGAAGAGAAAGGTC
S40R	CTTTGTAGGCAGCCGCTGCGGCAGCGACCTTTCTCTTCTTCTTTGG
S1-5e	AGG TTT GAA GGG GGA GTG ATT CAT CAA GTG TGT TAT GAA TTC GAG GGC TGA TCC G
IN3R	TGA CAC AGA AGT TCT CCT GAT GGA CCT CTT GCT TTT CCT GAA TCT TGT ATG
IN3F	CAT ACA AGA TTC AGG AAA AGC AAG AGG TCC ATC AGG AGA ACT TCT GTG TCA
S1-5R	CTC TCA TAG GGA ACA AGT GCA CCA T
Primers for qRT-PCR analysis:	
qFIS2F	TCGATTGGTGGTGGAGAATG
qFIS2R	AGTTACTGAGGAGGATGGTAGT
qFWAF	CGCCTTCTTCTTCCTCTAATCC
qFWAR	AGTCCACTTCTCCCAATGTAATC
ACT2F	GACCTTTAACTCTCCCGCTATG
ACT2R	GAGACACACCATCACCAGAAT
uUBCF	CTGCGACTCAGGGAATCTTCTAA
uUBCR	TTGTGCCATTGAATTGAACCC
qDMEc4F	GTGGTTGATCCGCTCAGTAA
qDMEc4R	CGTCCCTTTCATCTCTCGTAAA
qDMEc5F	GAGGAGAGGAGCTTAACAAGTG
qDMEc5R	TCTCCAACGGAAGAGGTAGT
qDMEc6F	CATCGTCTCCTTGATGGTATGG
qDMEc6R	CTTTCCCTCCACACTTCTGTT

Table S9. Average genomic coverage and DNA methylation for the samples in this study

Sample	Raw reads	Aligned bases	Average coverage	Chloroplast CHH methylation (%)
dme-2/dme-2; nDME^{CTD}-1/nDME^{CTD}-1	34935210	3746188650	15	0.3
dme-2/dme-2; nDME^{CTD}-2/nDME^{CTD}-2	38167678	4239339600	17	0.3
dme-2/dme-2; nDME^{CTD}-3/nDME^{CTD}-3	37046004	3999866100	16	0.3
dme-2/dme-2; DME^{FL}-1/DME^{FL}-1	22341056	2305678050	9	0.8
dme-2/dme-2; DME^{FL}-2/DME^{FL}-2	51293032	4850025750	19	0.4
dme-2/dme-2; DME^{FL}-3/DME^{FL}-3	39663046	4258662450	17	0.3

Chloroplast CHH methylation is an estimate of the bisulfite non-conversion rate in the sequenced samples.

References

1. Hehenberger E, Kradolfer D, & Kohler C (2012) Endosperm cellularization defines an important developmental transition for embryo development. *Development* 139(11):2031-2039.
2. Ibarra CA*, et al.* (2012) Active DNA demethylation in plant companion cells reinforces transposon methylation in gametes. *Science* 337(6100):1360-1364.
3. Hsieh TF (2015) Whole-genome DNA methylation profiling with nucleotide resolution. *Methods in molecular biology* 1284:27-40.
4. Frost JM*, et al.* (2018) FACT complex is required for DNA demethylation at heterochromatin during reproduction in Arabidopsis. *Proceedings of the National Academy of Sciences of the United States of America* 115(20):E4720-E4729.
5. Quinlan AR & Hall IM (2010) BEDTools: a flexible suite of utilities for comparing genomic features. *Bioinformatics* 26(6):841-842.
6. Sequeira-Mendes J*, et al.* (2014) The Functional Topography of the Arabidopsis Genome Is Organized in a Reduced Number of Linear Motifs of Chromatin States. *Plant Cell* 26(6):2351-2366.
7. Lyons DB & Zilberman D (2017) DDM1 and Lsh remodelers allow methylation of DNA wrapped in nucleosomes. *Elife* 6.